The Pennsylvania State University

The Graduate School

OPTIMAL LANDING TRAJECTORIES ON THE MOON USING LAMBERT TARGETING AND PARTICLE SWARM OPTIMIZATION

A Thesis in

Aerospace Engineering

by

Khushboo Bipinchandra Patel

Submitted in Partial Fulfillment
of the Requirements
for the Degree of

Master of Science

August 2019

The thesis of Khushboo Bipinchandra Patel was reviewed and approved* by the following:

David Spencer
Professor of Aerospace Engineering
Thesis Advisor

Robert Melton
Professor of Aerospace Engineering

Amy Pritchett
Professor of Aerospace Engineering
Head of the Department of Aerospace Engineering

*Signatures are on file in the Graduate School

ABSTRACT

This thesis presents a trajectory optimization problem for a lunar lander using Lambert's solution with a Particle Swarm Optimization method. The goal of this thesis is to look for optimal and repeatable transfers starting from a circular orbit to land at a desired location on the lunar surface.

The Particle Swarm Optimization method, inspired by the motion of birds swarming, has been used to find acceptable and appropriate solutions for low thrust trajectory transfers, small orbital maneuvers, investigating the shortest, propellant-efficient path for an airplane to go from one concentric circle to another, and flying multiple drones simultaneously. The purpose of this thesis is to determine the best location to start the descent to the Moon for multiple landings corresponding to the pre-selected landing site location. This research presents two cases where the cost function of the optimization problem with respect to various transfer variables of the trajectories is considered. The landing locations remain constant and a constant starting altitude of 100 km above the lunar surface is used. These cases represent two landing scenarios where the number of decision variables is either 1 or 3.

The elements investigated are the semi-major axis and eccentricity which define the shape of the trajectory, inclination of the transfer orbit with respect to the Moon's equatorial plane, right ascension of ascending node, true anomaly, the argument of periapsis and the time to land. The cost function for the optimization problem comprises the Δv_{Total} obtained by adding the two thrust velocities. The first thrust velocity is calculated by subtracting the velocity of the lander from the first Lambert's velocity to initiate descent and the second thrust velocity is evaluated by subtracting the second Lambert's velocity from the velocity needed to land at the site. Case I uses the time to land as the search space and therefore, sensitivity to initial conditions and the selection of a landing site remains higher than Case II. Case II uses a wider search space of the classical orbital elements that define the initial position of the spacecraft around the Moon and the time to land at a desired

landing site. Using Particle Swarm Optimization on Lambert's solution for a swarm of 100 trajectories, the ten local best trajectories are selected at each stage of the generation. The particle swarm optimization method was modified with an inclusion of simple genetic algorithm operators, crossover and mutation to increase interdependence between generations. These ten trajectories contain an effective combination of the decision variables that produces the lowest Δv_{Total}. This information is then utilized to generate the next swarm of 100 trajectories which is evaluated for fitness through Lambert targeting by Particle Swarm Optimization. Once the best solution does not change from generation to generation for around 50 generations for Case I and for 2000 generations for Case II, the ten best transfer trajectory characteristics with the lowest Δv_{Total} are recorded. These trajectory attributes include the pre-selected semi-major axis and inclination and a unique combination of the variables such as the right ascension of ascending node with respect to the Moon centered inertial coordinate system (MCI), true anomaly, the argument of periapsis and the time to land to complete the maneuver in minimum Δv_{Total}. This cost function in the form of Δv_{Total} directly corresponds to the propellant. The ten trajectories obtained through Case II are then used to generate ground tracks with respect to the lunar surface and appropriate downrange data are analyzed.

The process of Lambert targeting and Particle Swarm Optimization's randomness to produce initial conditions produces feasible results. Out of the possible solutions investigated, a circular orbit at 100 km altitude, inclined at 20° with the argument of latitude around 50° and a minimum propellant usage trajectory with Δv_{Total} of 1.723 km/s is found for landing at the "Sinus Medii" crater on the Earth-side of the Moon. The time-to-land calculated through the particle swarm optimization process for Case I is 41.46 minutes. Lower time-to-land for the corresponding Δv_{Total} were calculated by extending the search space in Case II to include a random combination of the right ascension of ascending node, the argument of latitude and the time-to-land in the particle swarm optimization process. At the end of several generations of a population of trajectories defined in classical orbital elements, the 10 best trajectories to attempt precise and

repeatable landings on the Moon are obtained. These trajectories produced a unique combination of the right ascension of ascending node Ω that defines the position of the ascending node of the transfer trajectory in the inertial frame and the argument of latitude *u* that defined the position of the lander itself on the orbit, for the selected initial altitude and inclination of the trajectory. Case II also produced optimal solutions for the minimum cost function Δv_{Total} for various combinations of classical orbital elements that increased the choice of landing trajectories within constraints. The only difference between Case I and Case II were the number of decision variables and although the values of optimal velocities obtained were lower than the Δv_{Total} at the beginning of the optimization process, sensitivity to the initial conditions used remained higher in Case I.

In summary, with the Particle Swarm Optimization, precise results with minimum propellant and via a Pareto frontier convergence curve for the cost function were obtained through many generations. The ten final trajectories obtained through this process can pave a way for multiple-precision landings on the Moon or a planetary surface.

TABLE OF CONTENTS

LIST OF FIGURES

LIST OF TABLES

Nomenclature

PSO: Particle Swarm Optimization	
MCI: Moon Centered Inertial frame	
MCMF: Moon Centered Moon Fixed rotating frame	
$\bar{r}_1$: Position vector of spacecraft before starting descent stage	km
$\bar{r}_2$: Position of the landing site on lunar surface	km
J : Total Δv required to make landing possible	km s^{-1}
T: Time to land on the lunar surface	s/min
a: Semi-major axis of the trajectory	km
e: Eccentricity	
i: Inclination of the orbit	rad/degree
Ω: Right ascension of ascending node	rad/degree
ω: Argument of perigee	rad/degree
θ: True anomaly	rad/degree
u: Argument of latitude	rad/degree
ϕ: Latitude	rad/degree
λ: Longitude	rad/degree
Ω_{Moon}: Angular velocity of Moon	rad s^{-1}
θ_{LST}: Local sidereal time angle	rad/degree
$\bar{\zeta}$: PSO variable vector	--
$\bar{\eta}$: PSO update variable vector	--
N: Number of trajectories in a Swarm	

ACKNOWLEDGMENTS

First and foremost, I would like to express my sincere gratitude and prayers to my ultimate teacher and Guru His Supreme Divine Holiness Pramukh Swami Maharaj to have inspired me to pursue my education at The Pennsylvania State University. Constant guidance, both academically and spiritually, from Him as well as from His Divine Holiness Mahant Swami Maharaj has led to the accomplishment of my education at Penn State. Furthermore, I would like to thank my parents Mr. Bipinchandra Patel and Mrs. Ritaben Patel for their endless support and motivation throughout my studies and in the process of preparing this thesis. Also, I would like to thank my grandmother Mrs. Ziniben Patel for believing in me and my brother Harsh for his support and care in my educational journey, far away from home.

It has been my honor to receive guidance from Dr. David Spencer, my advisor for this thesis. I would like to thank Dr. Spencer for his boundless patience throughout the topic exploration and constant direction which made this thesis possible from the fundamental level. Dr. Spencer has been my mentor since the undergraduate program and has helped me learn astrodynamics from basics.

I would like to extend my gratitude and appreciation to Dr. Melton for reviewing this thesis and our department head Dr. Amy Pritchett for the same. The acknowledgments section cannot be complete without a thank you to all my friends and colleagues at Penn State for reviewing the topic with me and for providing feedback. Throughout my time at Penn State, I have received guidance and support from great mentors and professors, and I would like to thank them all. Coming to Penn State and pursuing a degree in aerospace would not have been possible without the science and math concepts that I learned in school and therefore the acknowledgments section is incomplete without mentioning my teachers in primary, secondary and high school.

Finally, I would like to thank my grandfather the Late Mr. Bavabhai Patel who believed in me constantly and saw a vision which is still alive in our hearts.

Dedicated to my source of inspiration and my Guru His Supreme Divine Holiness Pramukh Swami Maharaj and His Holiness Mahant Swami Maharaj and my beloved parents,

Mr. Bipinchandra Patel and Mrs. Ritaben Patel.

Chapter 1

Introduction

Recently, a plethora of countries have discussed diverting funding to focus on Moon exploration, development of potential human habitation on Mars, and initiate manned missions for extended deep space exploration. In 2017, United States President Donald Trump signed the Space Policy Directive 1 with the revised National Space Policy to return to the Moon and reach Mars with effective collaboration between its commercial partners[1]. This created opportunities for commercial companies to compete for landers and other services to support space exploration, technology demonstrations, and science experiments under NASA's Commercial Lunar Payload Services (CLPS) program[2]. The Artemis missions to the Moon starting in 2020 also plan to put a man and the first woman on the Moon by 2024 as reported by NASA administrator Jim Bridenstine[3]. He further mentioned " President Donald Trump has asked NASA to accelerate our plans to return to the Moon and to land humans on the surface again by 2024. We will go with innovative new technologies and systems to explore more locations across the surface than was ever thought possible. This time, when we go to the Moon, we will stay. And then we will use what we learn on the Moon to take the next giant leap - sending astronauts to Mars. "Life support remains a crucial subsystem for such missions and thus the time as well as the propellant required for a mission needs to be balanced. Just like a flight plan map is needed for a cross country flight, all space missions require trajectories for the mission architecture. If humans plan to stay on the Moon and Mars, facilities need to be created in advance to support daily tasks and so to execute those, multiple trips to the Moon and Mars are inevitable. With efforts by Boeing, SpaceX, Blue Origin, other companies[5] and NASA to reduce the cost per launch[4], larger payloads need to be supplied and dropped close to the desired facility sites[2].

Multiple precision landings have been studied and implemented for years on Earth but never tested in space. Trajectory design helps engineers to visualize and control the small corrections, monitor fuel usage and move forward with the spacecraft design. Hazard avoidance is quite an essential part of the multiple and precision landings. Software like ALHAT (Autonomous Precision Landing and Hazard Avoidance Technology) help the guidance navigation system on board to evaluate the terrain, pass data through sensors, relay commands and make the final landing possible with available propellant[6]. Space travel comes with its various constraints, propellant, time, and safety to name a few. Optimal (minimum time or minimum propellant use) space trajectories have been researched over the years using various stochastic or deterministic optimization techniques[7].

Particle Swarm Optimization (PSO) is a stochastic algorithm used widely for global and local optimization methods[7]. The particle swarm optimization technique was first introduced by Kennedy and Eberhart in 1995 to optimize continuous non-linear functions[8]. PSO is inspired by the unpredictable motion of a swarm of birds searching for food and is comparable to ant-colony optimization. The birds fly together in flocks by sharing the information locally that leads to the overall global behavior of the swarm. This mechanism helps to optimize values of necessary unknown variables that have been used in space applications. In short, the solution is derived by cooperation and competition between the particles of a swarm. The initial population of the swarm is generated through the variables that affect the motion of the birds for the first iteration and then local position and velocity of individual particle that is the bird is updated using the local and global information. This is done using coefficients discussed further in the PSO section of this thesis, that eventually affects the convergence. The swarm is evaluated using a fitness function, which is a measure of some property or properties of each possible solution. The new population is generated stochastically, based on the fitness function.

Pontani and Conway[7] applied PSO as a technique for space trajectories and illustrated cases for applying constrained and unconstrained optimization for Lyapunov periodic orbits, impulsive transfer between two circular orbits and finite thrust orbital transfer between two circular orbits. Other papers in the literature also compare the PSO method with differential evolution algorithm[9]. Recently, a book by Couceiro and Ghamisi introduced particle swarm optimization as a solution to discontinuous, non-differentiable evolution and discussed the advantages and disadvantages for the same[10]. Pontani also collaborated with Ghosh and Conway to investigate PSO for multiple burn rendezvous trajectories[11] in 2012. PSO has also been applied to multistage launch vehicles[12] and for Mars atmospheric entry trajectories optimization along with a Gauss Pseudo-Spectral method[13].

The goal of this thesis is to apply a particle swarm intelligence technique for finding optimal landing locations on the Moon and other planets by optimizing the velocity needed to start the descent at a suitable starting location. Since the swarm of trajectories comprises information on the initial position of the lander and the desired landing location is known, and the approximate time to land is evaluated, Lambert's solution[15] using a universal variable approach is used to calculate the cost function Δv_{Total} of this optimization process. In addition, this thesis investigates the possible optimal starting trajectories to reach desired landing locations on the surface of the Moon with a minimum amount of propellant, thereby making multiple precision landings possible. This thesis begins with the introduction of the theory and principles that are combined to perform optimization through Lambert targeting. Chapter 3 follows with the procedures for Lambert targeting with PSO while also presenting the assumptions in orbital dynamics and the two main cases considered. Chapter 4 discusses the findings of the simulated cases. Chapter 5 provides a sensitivity analysis of the decision variables for each case that are explained in detail in Chapter 2 and their corresponding results. Chapter 6 provisions a conclusion statement providing information on potential landing locations and the corresponding initial conditions for each case considered to start the descent.

Chapter 2

2.1 Problem Formulation

The objective of this thesis is to find optimal trajectories on the Moon to land at the desired landing location, starting from an initial orbit. This is done by introducing an unconstrained optimization problem to minimize the cost function, Δv_{Total}, which is the total velocity required in the form of engine burns to reach the landing location, starting from an initial circular orbit around the Moon. The optimization method used is the particle swarm optimization (PSO) and the orbit determination technique used is the Lambert's solution. The goal of this optimization process is to minimize Δv_{Total} calculated through Lambert's targeting. The search space variables are the classical orbital elements that defines the orbit's shape, size and orientation and the time-to-land on the Moon. This is an unconstrained optimization with a cost function that uses the ranges defined for the search space variables to find the optimal trajectory characteristics after several iterations. Note that, for this thesis, PSO was modified to transition from one iteration to another for stability in convergence and details of the operations used are included in section 3.2 of Chapter 3.

This chapter introduces the theory, variables, and equations used for the research. Additional information on the application of Particle Swarm Optimization to Lambert's problem is included in Chapter 3.

2.2 Mathematical and Physical Principles

Observation is an essential part of space mission planning and hence, depending on the preliminary orbital parameters, appropriate orbital determination techniques must be used[14]. Since this is a landing phenomenon, juxtaposing two known position vectors and the approximate time of flight between them help determine the initial and terminal velocities and so Lambert's problem

of initial orbital determination is used. Lambert's Algorithm to calculate lambert velocities using the universal variable approach, from Curtis[15] as well as Vallado[14], is used while the coordinate transformation algorithms are adopted from Vallado[14]. The following sections include details on Lambert's problem and PSO.

2.2.1 Lambert's problem

The two-body boundary value problem, called Lambert's problem, is used extensively in astrodynamics analysis. Lambert, a French-born German astronomer, physicist and mathematician developed the theory in 1761. The theory determines where a trajectory can be defined given initial position $\bar{r}_1$ and the final position $\bar{r}_2$ of one body moving with respect to another[14]. According to Vallado, the original Lambert's formulation uses eight cases to conclude a final answer and other solutions like universal variable solution and algorithms by Battin[25] (1987) or Thorne's direct solution are also developments in the literature[14]. The theory presented here follows Curtis and Vallado's universal variable approach which can be applied to all conic sections.

In this case, the Moon is the principal mass and the spacecraft is revolving at a certain initial orbit around the Moon. The goal of this research is to find a suitable departure descent point P_1 to enable minimum velocity change (Δv_{Total}) and propellant usage to reach a latitude/longitude location point P_2 on the surface of the Moon. This velocity change, Δv_{Total} is defined as the total velocity in the form of engine burns, required to reach point P_2 from P_1. Equations used for this analysis to calculate Δv_{Total} are included later in this section. Lambert's problem illustration is depicted in Fig. 2.1 from Curtis[15].

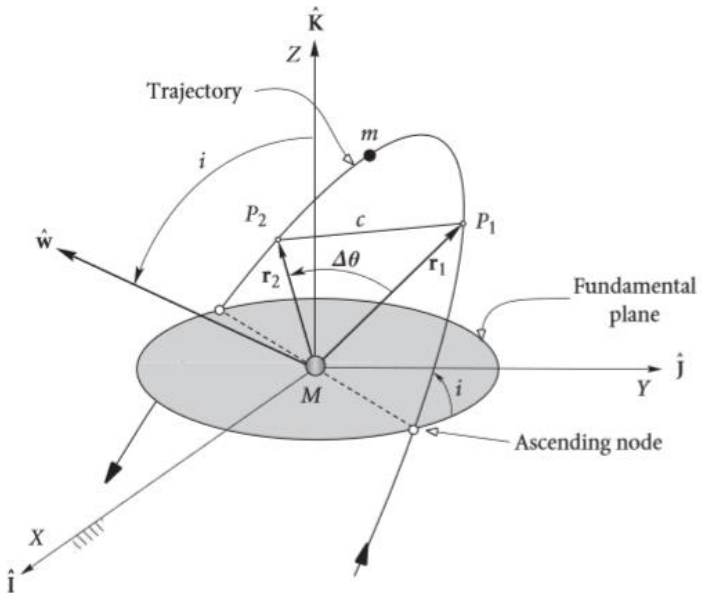

Figure 2.1: Description of positions and coordinate axes for Lambert's problem. (Curtis[15])

The change in true anomaly for this two impulse maneuver is determined by Eq. (2.1) where r_1 and r_2 are the magnitudes of the position vectors $\bar{r}_1$ and $\bar{r}_2$ of the spacecraft before the descent and at the landing location respectively.

$$cos\Delta\theta = \frac{\bar{r}_1 \bar{r}_2}{r_1 r_2} \tag{2.1}$$

Note that for this research the inertial reference frame is the Moon centered inertial (MCI) reference frame indicated in Fig 2.2. When the Moon rotates with respect to an observer on Earth, the Moon fixed rotational frame (MCMF) moves with it. Thus, the difference between the Moon fixed inertial coordinate frame and the Moon rotational frame is the angular velocity of the Moon which is calculated as $\Omega_{moon} = 2.66 \times 10^{-6}$ rad/s or one revolution per lunar month, 27.3217 days. For simplicity in calculations, the inclination of the Moon's elliptical orbit around the Earth's equatorial plane is considered zero.[17] Prime meridian on the lunar surface is considered as the zero longitude point, and hence there is negligible difference between the values of the right ascension

from the topocentric coordinate frame and east longitude. For this thesis, east longitude is considered positive, and other positions are indicated in Fig 2.2.

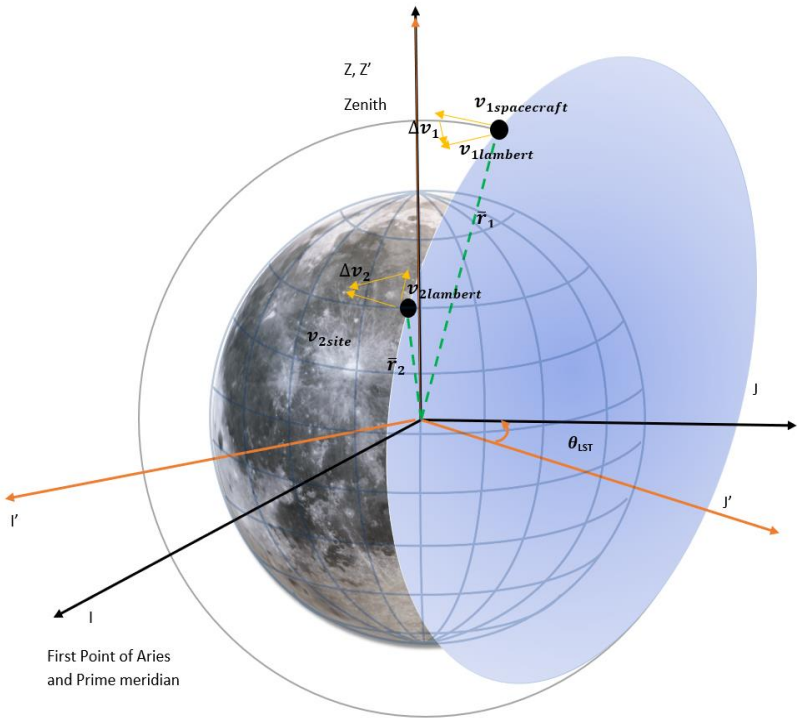

Figure 2.2: Coordinate systems diagram and the position of P_1 and P_2.

The MCI coordinate system's origin is also the center of the Moon and the MCMF rotates with the Moon with angular velocity Ω_{moon}. Point P_1 is located at an altitude 100 km above the surface of the Moon with associated $\bar{r}_1$ and point P_2 is located with the corresponding position $\bar{r}_2$ and the velocity vectors illustrated in Fig 2.2. If the initial descent point P_1, the landing location point P_2 and the time of flight between them is given, Lambert's problem determines an appropriate trajectory between the two points. This time of flight will also be the decision variable in the two cases presented in Chapter 3. According to Lambert's theorem, the transfer time from P_1 to P_2 depends only on the sum of r_1 and r_2, semi major axis of the ellipse passing through the two points

and the length of the chord line c joining P_1 and P_2. Figure 2.3 illustrates qualitatively the objective of this thesis which is to reach landing locations from variable initial positions in orbit.

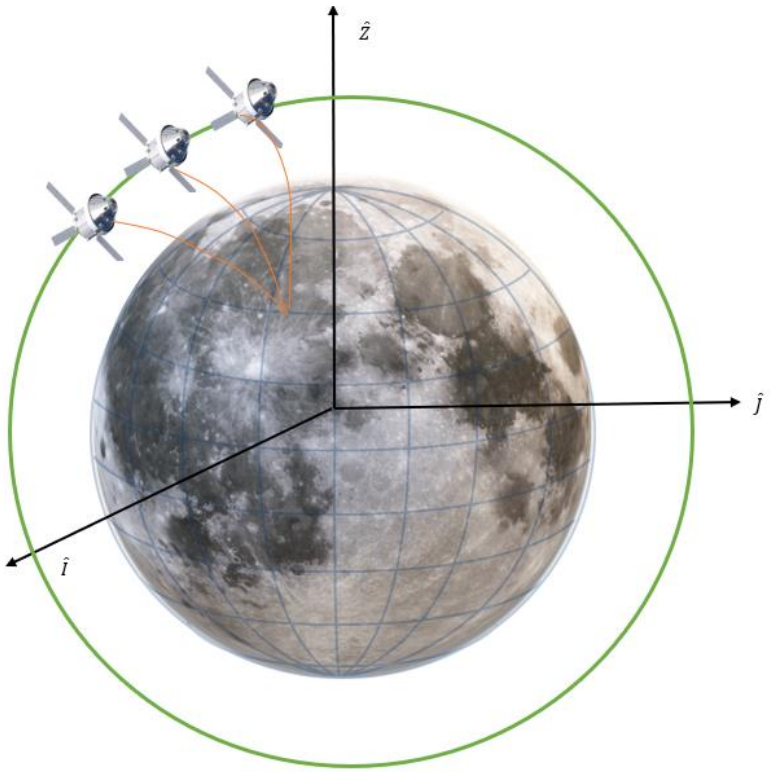

Figure 2.3: Graphical demonstration of multiple landings on the Moon.

Universal anomaly equations are used to calculate the radius and velocity at a later time in Lambert's problem[14]. The universal anomaly helps to identify any hyperbolic or parabolic transfer trajectories generated during large computations and provide appropriate filters. Another advantage of using universal variables is that they permit calculation of the Lagrange coefficients while accounting for all four conic sections without having to apply different eccentric anomaly iterations to the problem. Lagrange coefficients appear in Eqs. (2.4) through (2.8) and are used to relate the first position vector to the second position vector and to the velocity vectors. The universal anomaly χ along with the Stumpff functions *C(z)* and *S(z)* are used to analyze orbits and the Eqs. (2.2) and (2.3), included further in this section illustrate the relations where $z = \alpha\chi^2$ and $\alpha = \frac{1}{a}$.

$$S(z) = \sum_{k=0}^{\infty} \frac{(-1)^k z^k}{(2k+3)!} = \frac{1}{6} - \frac{z}{120} + \frac{z^2}{5040} - \frac{z^3}{362{,}880} + \cdots \tag{2.2}$$

$$C(z) = \sum_{k=0}^{\infty} \frac{(-1)^k z^k}{(2k+2)!} = \frac{1}{2} - \frac{z}{24} + \frac{z^2}{720} - \frac{z^3}{40{,}320} + \cdots \tag{2.3}$$

Finding orbital elements requires either the initial state $\bar{r}_1$ and $\bar{v}_1$ or the final state $\bar{r}_2$ and $\bar{v}_2$, which are related by Lagrange coefficients as illustrated in Eq. (2.4), Eq. (2.5) and Eq. (2.6). In this thesis, $\bar{r}_1$ represents the initial radius vector of the starting trajectory of the spacecraft having velocity $\bar{v}_1$ that is needed to land at point P_2 with vector $\bar{r}_2$ and velocity $\bar{v}_2$.

$$\bar{r}_2 = f\,\bar{r}_1 + g\bar{v}_1 \tag{2.4}$$

$$\bar{v}_2 = \dot{f}\,\bar{r}_1 + \dot{g}\bar{v}_1 \tag{2.5}$$

$$\bar{v}_1 = \frac{1}{g}(\bar{r}_2 - f\bar{r}_1) \tag{2.6}$$

It should be noted that $z < 0$ for hyperbolic trajectories, $z = 0$ for parabolic orbits and $z > 0$ for elliptical orbits. Lagrange coefficients are independent of eccentricity. Thus, Eqs. (2.7a), (2.7b), (2.7c) and (2.7d) express them in terms of universal anomaly χ and Eqs. (2.8a), (2.8b), (2.8c) and (2.8d) express the coefficients in terms of $\Delta\theta$.

$$f = 1 - \frac{\chi^2}{r_1}\ C(z) \tag{2.7a}$$

$$g = \Delta t - \frac{1}{\sqrt{\mu}}\chi^3\, S(z) \tag{2.7b}$$

$$\dot{f} = \frac{\sqrt{\mu}}{r_1 r_2} \chi \ [z\, S(z) - 1] \tag{2.7c}$$

$$\dot{g} = 1 - \frac{\chi^2}{r_2} \ C(z) \tag{2.7d}$$

$$f = 1 - \frac{\mu r_2}{h^2} \ (1 - \cos \Delta\theta) \tag{2.8a}$$

$$g = \frac{r_1 r_2}{h} \sin \Delta\theta \tag{2.8b}$$

$$\dot{f} = \frac{\mu}{h} \ \frac{1 - cos\Delta\theta}{\sin \Delta\theta} \ \left[\frac{\mu}{h^2} \ (1 - \cos \Delta\theta) - \frac{1}{r_1} - \frac{1}{r_2}\right] \tag{2.8c}$$

$$\dot{g} \ = \ 1 - \frac{\mu r_1}{h^2} \ (1 - \cos \Delta\theta) \tag{2.8d}$$

By solving the Eqs. (2.7) and (2.8) and using the fact that $f\dot{g} - \dot{f}g = 1$, the unknown angular momentum is solved using Eq. (2.9). Also equating $\dot{g}$ from Eqs. (2.7d) and (2.8d), yields the expression for *A* in Eq. (2.10) used later to find the relation between *z*, χ and the time interval, iteratively using Newton's method applied to the function *F(z)*.

$$h = \sqrt{\frac{\mu r_1 r_2 (1 - \cos \Delta\theta)}{\chi^2 C(z)}} \tag{2.9}$$

$$A = \sin \Delta\theta \sqrt{\frac{r_1 r_2}{1 - \cos \Delta\theta}} \tag{2.10}$$

$$\chi = \sqrt{\frac{y(z)}{C(z)}} \tag{2.11}$$

$$y(z) = r_1 + r_2 + A \ \frac{z\, S(z) - 1}{\sqrt{C(z)}} \tag{2.12}$$

$$F(z) = \left[\frac{y(z)}{C(z)}\right]^{\frac{3}{2}} S(z) + A \sqrt{y(z)} - \sqrt{\mu}\, \Delta t \tag{2.13}$$

$$F'(z) = \frac{dF(z)}{dz} = \begin{cases} \left[\frac{y(z)}{C(z)}\right]^{\frac{3}{2}} \left\{\frac{1}{2z}\left[C(z) - \frac{3}{2}\frac{S(z)}{C(z)}\right] + \frac{3}{4}\frac{S(z)^2}{C(z)}\right\} + \frac{A}{8}\left[\frac{3\,S(z)}{C(z)}\sqrt{y(z)} + A\sqrt{\frac{C(z)}{y(z)}}\right] & z \neq 0 \\ \left[\frac{\sqrt{2}}{40}y(0)^{3/2} + \frac{A}{8}\left[\sqrt{y(0)} + A\sqrt{\frac{1}{2y(0)}}\right]\right] & z = 0 \end{cases} \tag{2.14}$$

$$C(z) = \begin{cases} \frac{1-\cos(\sqrt{z})}{z} & z > 0 \\ \frac{\cosh\sqrt{-z}-1}{-z} & z < 0 \\ \frac{1}{2} & z = 0 \end{cases} \tag{2.15}$$

$$S(z) = \begin{cases} \frac{\sqrt{z} - \sin(\sqrt{z})}{\sqrt{z^3}} & z > 0 \\ \frac{\sinh\sqrt{-z} - \sqrt{-z}}{\sqrt{-z^3}} & z < 0 \\ \frac{1}{6} & z = 0 \end{cases} \tag{2.16}$$

Equations (2.15) and (2.16) illustrate the values of Stumpff functions for different values of *z* used in Curtis[15] and Vallado's universal variable approach for Lambert[14]. At the beginning of the Lambert algorithm[15], the value of *z* is guessed and then Newton's method (Eq (2.17)) iterates and evaluates the final value of *z* using some tolerance.

$$z_{i+1} = z_i - \frac{F(z_i)}{F\prime(z_i)} \tag{2.17}$$

After evaluating *z* and the corresponding *y(z)* and *F(z)*, Lagrange coefficients are evaluated using Eqs. (2.18a), (2.18b), (2.18c) and (2.18d) that leads to the two Lambert velocities solved by Eqs. (2.19) and (2.20).

$$f = 1 - \frac{y(z)}{r_1} \tag{2.18a}$$

$$g = A\sqrt{\frac{y(z)}{\mu}} \tag{2.18b}$$

$$\dot{f} = \frac{\sqrt{\mu}}{r_1 r_2}\sqrt{\frac{y(z)}{C(z)}}[z\,S(z) - 1] \tag{2.18c}$$

$$\dot{g} = 1 - \frac{y(z)}{r_2} \tag{2.18d}$$

The total Δv for the maneuver is calculated by first adding the magnitude of the vector difference between the first velocity $\bar{v}_{1Lambert}$ obtained from Lambert's solution and the magnitude of $\bar{v}_{2Lambert}$. Thereafter, the magnitude of the velocity vector difference between the velocity needed to land at the site, denoted as $\bar{v}_{2site}$ and the velocity of the spacecraft at point P_1 before starting the descent denoted as $\bar{v}_{1spacecraft}$, is added to obtain Δv_{Total}. This is evident in Eqs. (2.21) and (2.22) and illustrated in Fig. 2.2. Note that $\bar{v}_{2site}$ is calculated by using latitude and longitude of the landing site, converting that into position and velocity coordinates in MCMF frame related by the angular velocity of the Moon and then converting it to MCI frame for Lambert's algorithm. Equations for converting latitude and longitude to $\bar{v}_{2site}$ in MCI frame are included in Chapter 3. A full version of the optimization algorithm with coordinate transformation and Lambert's targeting is included in the Appendix.

$$\bar{v}_{1Lambert} = \frac{\bar{r}_2 - (f\,\bar{r}_1)}{g} \tag{2.19}$$

$$\bar{v}_{2Lambert} = \frac{\bar{r}_2\dot{g} - \bar{r}_1}{g} \tag{2.20}$$

$$\Delta v_1 = \left|\bar{v}_{1Lambert} - \bar{v}_{1spacecraft}\right| \tag{2.21a}$$

$$\Delta v_1 = |\bar{v}_{2site} - \bar{v}_{2Lambert}| \qquad (2.21b)$$

$$J = \Delta v_{Total} = \Delta v_1 + \Delta v_2 \qquad (2.22)$$

The lunar surface, in this analysis, is assumed to have a perfect circular shape and hence, other perturbations, gravitational potential and terrain features are ignored for the simulation. Location of the landing site is preselected by considering previous landing sites and suitable-surface craters, not considered to scale. If this optimization is performed for landing at other planetary surfaces, an appropriate atmospheric model and other constraints need to be included in the equations. All computations for the Lambert's solution for this research are done using MATLAB R2018a. Further details on the steps or values used for the computations are included in Chapter 3.

2.2.2 Particle Swarm Optimization

Nature-inspired engineering has been contributing to finding innovative solutions to our daily problems. Out of many algorithms developed from interpretations of the movement of organisms, particle swarm optimization has gained popularity in optimizing space trajectories. It is closely related to genetic algorithms and evolutionary computations while also being computationally inexpensive with memory allocation. PSO is different than a genetic algorithm where individuals retain part of their identities while the process of destruction of previous information occurs. As explained by Kennedy and Eberhart[8], particle swarm optimization imitates birds' social behavior. The birds in a swarm that represents the particles in the PSO algorithm store individual information leading to the local best solution called the fitness function and then interact with the group to obtain the global best solution to the fitness function. As discussed before,

research has been done for decades especially by Pontani and Conway [7, 11, 12] towards optimizing trajectories in space.

The research performed in this thesis compares each bird in a swarm to a spacecraft trajectory that needs to land on the Moon. To continue space exploration for when a habitat on the Moon or Mars is a reality, multiple landings on the lunar surface becomes necessary. Furthermore, payloads need to be dropped off close to one another to reduce the time travel for retrieval of mission parts with limited propellant onboard which points towards optimized solutions. Many numerical optimization techniques that exist are either deterministic or heuristic. As mentioned before, heuristic methods are based on Darwin's principle of survival of the fittest through evolution. The gradient-based deterministic methods, for continuous functions only, are strongly dependent on initial conditions or strong identification of first attempt solution. This is where evolutionary algorithms work better where new individuals are created using old individuals and reach convergence for an objective function. Birds in a swarm fly together, search for food together and land together without collisions and the flocking behavior incorporated through PSO is the inspiration for the optimization method used in the current thesis.

The goal is to find possible best solutions for starting trajectories through many possible combinations of trajectory constraint combinations while also minimizing the total Δv for the maneuver. By starting with some initial trajectory characteristics, PSO is used to find the best trajectory to connect a descent point P_1 on the initial trajectory to a landing site point P_2. Lambert's algorithm calculates the velocities needed for the maneuver while PSO finds the best solution through several iterations and survival of the fittest trajectories. The theory behind PSO is that each particle in a population is assigned an instantaneous individual position $\bar{x}$, moving with a velocity $\bar{v}$ through the search space. This position is updated at a time *(t+1)* using the relation between previous position and velocity that is now a combination of the particle's individual information and the swarm information, represented by $\bar{v}_{i(t+1)}$ and as illustrated in Eqs. (2.23) and (2.24).

Coefficients w , C_1 and C_2 represent the inertial component, cognitive or personal component and social component of the update velocity vector $\bar{v}_{i(t)}$. P_i corresponds to the local best value of the position $\bar{x}$ and g_i corresponds to the global best. At each iteration, local best and global best values are compared to the previous local and global values leading to optimal values. Note that the dimensions of $\bar{x}$ and $\bar{v}$ are the same and do not represent position and velocity as physical quantities.

$$\bar{x}_{i(t+1)} = \bar{x}_{i(t)} + \bar{v}_{i(t+1)} \tag{2.23}$$

$$\bar{v}_{i(t+1)} = w\bar{v}_{i(t)} + C_1\left(P_{i(t)} - \bar{x}_{i(t)}\right) + C_2\left(g_{i(t)} - \bar{x}_{i(t)}\right) \tag{2.24}$$

Equations (2.23) and (2.24) represent the particle swarm update for one iteration. This process continues for the number of iterations throughout the search space to optimize the cost function. Correlating that to the purpose of this thesis, optimization is done using a search space containing classical orbital elements starting with semi-major axis a, eccentricity *e*, inclination *i*, right ascension of ascending node **Ω**, argument of periapsis ω and true anomaly θ that defines trajectories in inertial space along with the time-of-flight T. The classical orbital elements represent the information $\bar{x}$ from Eq. (2.23) at a time which is updated through $\bar{v}$, as the trajectory progresses in time. For circular orbits, θ is undefined and so the argument of latitude u= ω+ θ, is used and for equatorial orbits, true longitude l= θ + (ω + **Ω**) is used. The fitness function J is the Δv_{Total} that results from Lambert's solution discussed before. This analysis uses a particle swarm optimization technique on Lambert's solution to find the best combination of trajectories defined by classical orbital elements starting at the descent point P_1 to reach a landing location point P_2 on the Moon.

For effective sensitivity analysis of variables and to conclude with the stochastic algorithm, PSO is applied to two cases defined later in Chapter 3, involving a vector variable that contains the

classical orbital elements, defining the starting trajectories and the time-of-flight T that makes the landing possible. The variable vector is defined as $\bar{\zeta}$ with {a e i Ω ω θ T } unknown parameters which represent $\bar{x}$ from Eq. (2.23) and the update variable is defined as $\bar{\eta}$ that represents $\bar{v}$ from Eqs. (2.23) and (2.24). The optimization in this research has been treated as unconstrained optimization because the unknown parameters in $\bar{\zeta}$ have constrained ranges but no relative termination statement is applied during the computation.[18] Instead, values of the cost function Δv_{Total} are analyzed to record changes in Δv_{Total} from iteration to iteration and when the difference is more than 0.001 through more than 20 generations, the optimal values are accepted. From this point onwards the particles in a swarm in PSO will be stated as 'trajectories in a swarm'.

Each particle represents a trajectory i (i = 1,…, N) in a swarm of N particles and is associated with a search space position vector also called the variable vector $\bar{\zeta}(i)$ and the update variable vector $\bar{\eta}(i)$. Constraints on the variable vector are defined as $\alpha_k \leq \zeta_k \leq \beta_k$ where k=1,..,7 and on update variable as $-(\beta_k - \alpha_k) \leq \eta_k \leq (\beta_k - \alpha_k)$. This is to ensure that η_k does not violate the range at each new iteration. Equations. (2.24) and (2.25) illustrates the PSO variables applied to this thesis, subject to constraints defined in Eq. (2.26). Time dynamic evolution of these variables with PSO lead to convergence of fitness function J from Eq. (2.22) in Lambert's solution.

$$\bar{\zeta}_i^j = [a_i \;\; e_i \;\; i_i \;\; \Omega_i \;\; \omega_i \;\; \theta_i \;\; T_i] \tag{2.24a}$$

$$\bar{\zeta}_{i(t+1)}^j = \bar{\zeta}_{i(t)}^j + \bar{\eta}_{i(t+1)}^j \tag{2.24b}$$

$$\bar{\eta}_{i(t+1)}^j = C_I \bar{\eta}_{i(t)}^j + C_C \left(\bar{\eta}_{i(localbest)}^j - \bar{\zeta}_{i(t)}^j\right) + C_S \left(\bar{\eta}_{i(globalbest)}^j - \bar{\zeta}_{i(t)}^j\right) \tag{2.25}$$

$$\alpha_k \leq \zeta_k \leq \beta_k \qquad and \qquad -(\beta_k - \alpha_k) \leq \eta_k \leq (\beta_k - \alpha_k) \tag{2.26}$$

The inertial coefficient C_I, cognitive C_C and social C_S coefficients have the expressions[7] shown in Eqs. (2.27a), (2.27b) and (2.27c). Each trajectory *i*, has information $\bar{\zeta}_{i(t)}^{j}$ moving with $\bar{\eta}_{i(t)}^{j}$ at initial time *t* and at generation *j* through the algorithm. This translates to point P_1 having information $\bar{\zeta}(0)$ at time *t* in the form of classical orbital elements and the time-to-land. After time *t = t+1*, that is at a new generation, the trajectory has new information with $\bar{\eta}_{i(t+1)}^{j}$ that also contains the local best value of velocity variable $\bar{\eta}_{i(localbest)}^{j}$ and global best $\bar{\eta}_{i(globalbest)}^{j}$ upto that generation as evident from Eq.(2.25). Therefore, information of the classical orbital elements and time-of-flight T defining $\bar{r}_1$ and $\bar{v}_{1spacecraft}$ of the trajectory in a swarm is updated using Eq. (2.24b) at j^{th} generation. The initial swarm or population of N trajectories for this problem is stochastically generated between search spaces defined in Eq. (2.26). The maximum number of generations or iterations, j_{max} are decided based on the optimal lowest value of the cost function J that is Δv_{Total} and to avoid false convergence. The coefficients C_I, C_C and C_S play an important role in deciding the weightage of the personal best, local best or the global best values of the variables. $r_1(0,1)$, $r_2(0,1)$ and $r_3(0,1)$ are independent uniformly distributed random numbers between 0 and 1. Sensitivity of these coefficients to the optimal solutions will be covered in Chapter 5.

$$C_I = \frac{1 + r_1(0,1)}{2} \tag{2.27a}$$

$$C_C = 1.49445\, r_2(0,1) \tag{2.27b}$$

$$C_S = 1.49445\ r_3(0,1) \tag{2.27c}$$

Chapter 3

Particle Swarm Optimization Method Application to Lambert's Solution

3.1 Approach

This section introduces the plan for Lambert's targeting using particle swarm optimization. First, a population/swarm of N starting trajectories for P_1 as shown in Fig 3.1, are generated using a random function feature of MATLAB for parameters in $\bar{\zeta}$. The swarm size, i.e. the value of N, is selected as 100 for simplicity in matrix creation and multiplication. The seven variables are a, *e*, *i*, **Ω**, ω, θ and T and the range of values specified for each, satisfy the characteristics of a circular orbit around the surface of the Moon. The values for the right ascension of ascending node, aligning with the x-axis of the Moon inertial coordinate system range from [0° 360°], ω is 0°, e is 0 and true anomaly corresponding to the argument of latitude is [0° 360°]. For the variables used in each case presented in this section, inclination is selected from the range [0° 180°]. Time-of-flight or the time-to-land represented by T starts at 0 and generates 100 random values of T that do not go above the period of the initial circular orbit (7066 seconds), arbitrarily chosen to have an altitude of 100 km around the Moon. This gives the 100 starting variables for point P_1 defined by $\bar{r}_1$ by converting classical orbital elements to Cartesian coordinates in the MCI frame.

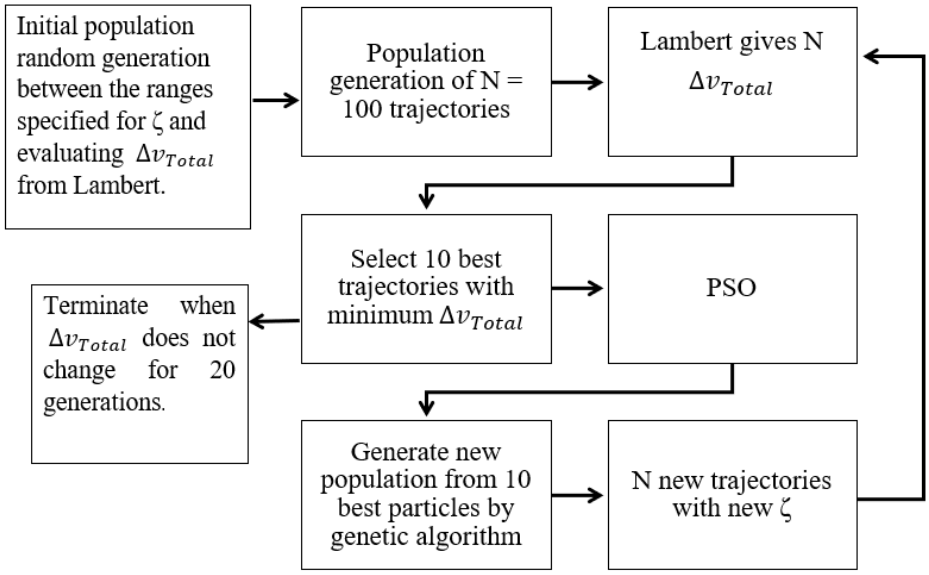

Figure 3.1: Lambert targeting by Particle Swarm Optimization flowchart

For point P_2, the landing site coordinates are created using λ, ϕ, and θ_{LST} through Eq. (3.1) in MCMF frame which is then converted to the inertial MCI frame by using Eq. (3.2). This is illustrated in Fig. 3.2 and θ_{LST} is calculated from T and Ω_{Moon} by Eq. (3.3).

$$\bar{r}_{2(MCMF)} = \begin{bmatrix} R_{moon}\,(\cos\phi\ \cos\lambda) \\ R_{moon}\,(\cos\phi\ \sin\lambda) \\ R_{moon}\,(\sin\phi) \end{bmatrix} \begin{bmatrix} \hat{I}' \\ \hat{J}' \\ \hat{K}' \end{bmatrix} \tag{3.1}$$

$$\bar{r}_2 = \begin{bmatrix} -\cos\theta_{LST} & -\sin\theta_{LST} & 0 \\ \sin\theta_{LST} & -\cos\theta_{LST} & 0 \\ 0 & 0 & 1 \end{bmatrix} \bar{r}_{2(MCMF)} \begin{bmatrix} \hat{I} \\ \hat{J} \\ \hat{K} \end{bmatrix} \tag{3.2}$$

$$\theta_{LST} = \Omega_{moon}\, T \tag{3.3}$$

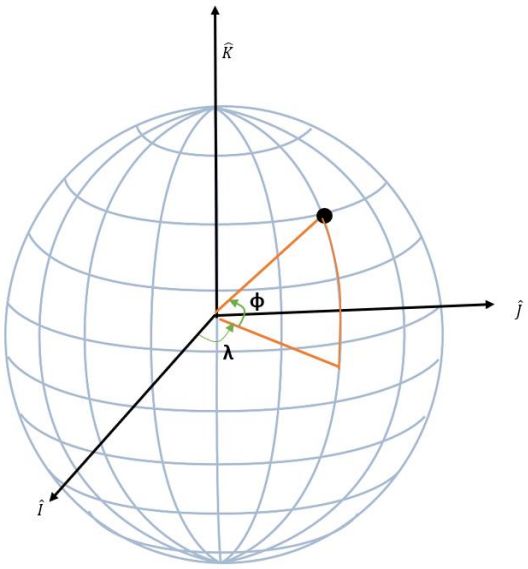

Figure 3.2: Latitude and Longitude of the Landing site in MCI

The 100 different position vectors $\bar{r}_1$ and $\bar{r}_2$ and the time-to-land T uses the Lambert's Algorithm discussed in Chapter 2, to calculate the suitable $\bar{v}_{1Lambert}$ and $\bar{v}_{2Lambert}$ which in return calculates the Δv_{Total} in km/s using Eq. (2.21) and (2.22). The significance of Δv_{Total} for this two impulse maneuver is related to the rocket equation that determines the propellant usage. Δv_{Total} is also the cost function J for the PSO algorithm that is evaluated for fitness. The next step in this process, as evident from Fig. 3.1, involves sorting the particles according to the ascending order of J and selecting the 10 best. Equations (2.25) to (2.27) are used to update the 10 best $\bar{\zeta}$ of the 10 selected trajectories. These 10 are the feed for the creation of the next swarm or the trajectory population that uses simple mutation and crossover to create new N trajectories defined in the search space. The next generation is created by genetic algorithm operators, crossover and mutation. Note that, PSO is used for optimizing the cost function while searching for global and

local minimum and genetic algorithm operators are used only to move from one generation to another generation.

Crossover is defined as the process of creating offspring population from the parent population by recombination of information between the parent population. Mutation is also an operator in an evolutionary computation that generates offspring population by introducing diversity between the parent population and offspring populations. This occurs by altering some values of the offspring population in the iteration compared to the initial iteration[26]. Both are used for this thesis and it is because when the 100 trajectories evaluate minimum Δv_{Total}, those ten trajectories are carried through generations until a new fit trajectory with lower Δv_{Total} than the Δv_{Total} of the previous trajectory is obtained. These trajectories having new $\bar{\zeta}$ are utilized to calculate the new J using constant $\bar{r}_2$ and evaluated for fitness until the cost function converges after several generations. The definition of convergence of J is that it stops changing generation after generation within some small tolerance for at least 20 generations and that minimum of J is recorded as $J_{Optimal}$. These trajectory characteristics can be used to attempt repeatable landings on the Moon and other interplanetary surfaces in the future. Figure 3.3 is a generalized diagram for the processes indicated in Fig. 3.1. After the PSO update, keeping the 10 best, the other 90 trajectories for the new population are generated by using uniform distribution random function between the ranges defined for the variables. At this point, genetic algorithm operators are introduced to add interdependence between the old generation and the new generation. The crossover point is 10 because the best ten are kept and the remaining 90 trajectories are created at the end of one generation. The 90 created trajectories along with the best ten trajectories are the feed for the new generation. After the new population is generated, Lambert is used to evaluate the cost function J and to find the global minimum by comparing all 100 trajectories. For better analysis, this approach uses two cases in the form of landing scenarios to discuss the seven unknown variables and their contribution to the optimization.

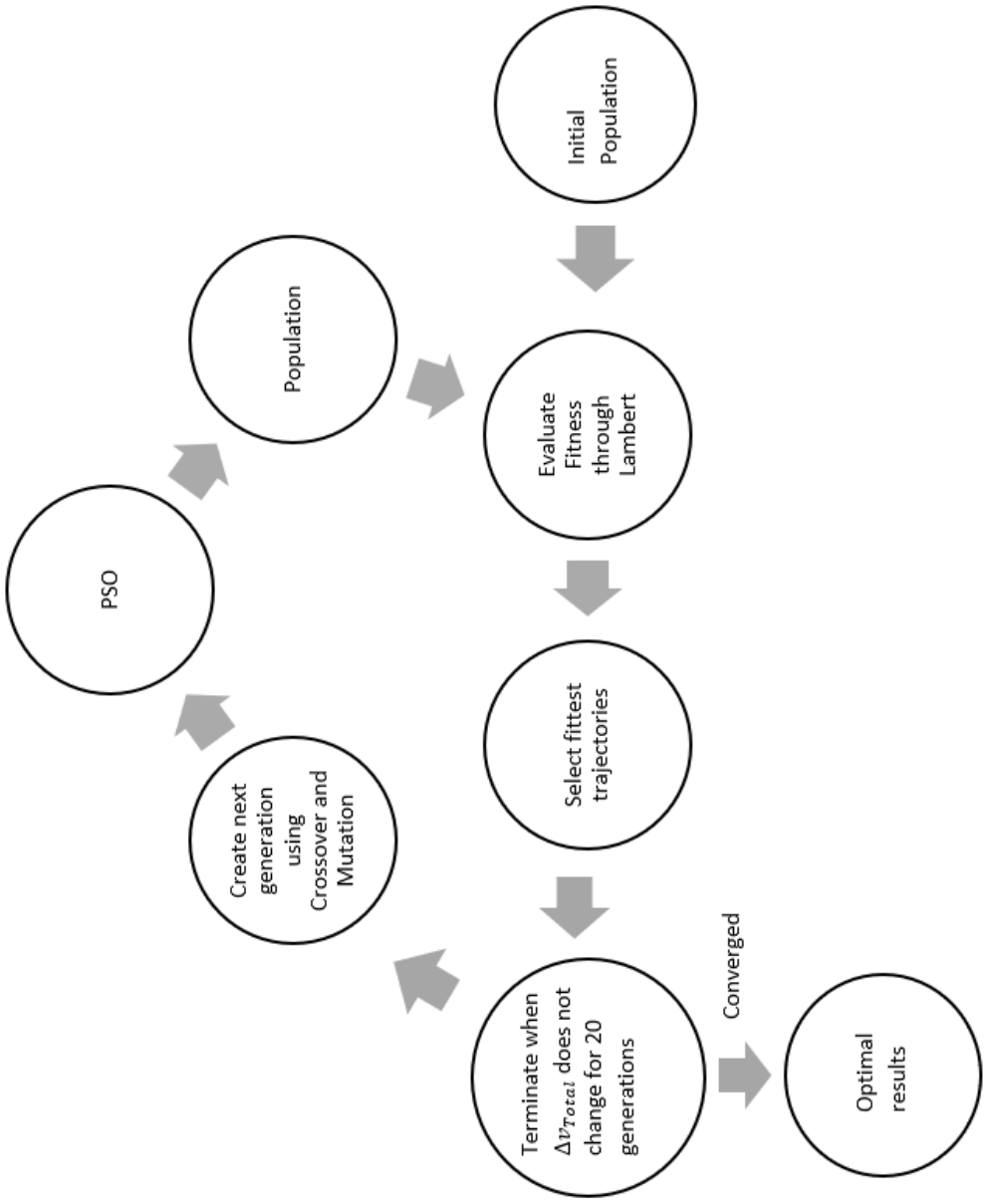

Figure 3.3: Interaction of the swarm with PSO and usage of genetic algorithm operators.

3.2 Cases

3.2.1 Case I: Time-to-Land *T* as a Variable

The spacecraft is in a circular orbit around the Moon at an altitude of 100 km. It is finding a location to land but needs to find at least 10 suitable solutions to initiate the landing. The initial value of $\bar{\zeta}_i^1 = [1837.4\,km \;\; 0 \;\; 0° \;\; 0° \;\; 0° \;\; 0° \;\; T_i]$ is used. Values for time to land are generated through a uniform distribution between the range of 0 s to 7000 s. Landing site coordinates are defined by latitude ϕ, longitude λ and Local Sidereal Time angle θ_{LST}. Using the rotational velocity of the Moon denoted as Ω_{Moon} and the N values of T, an initial swarm of 100 trajectories is created for a landing site. The values of latitudes and longitudes are created between ϕ = [0° 90°] and λ = [0° 90°]. The initial swarm has local best and global best values corresponding to the minimum *J* in the population. The goal of this case was to find the best *J* and corresponding *T* after a maximum of 250 generations. The definition of convergence for this case is that the change in *J* per generation should be less than 10^{-3}. The case also investigates the behavior of the swarm for different values in inclination *i*, right ascension of ascending node Ω and the argument of latitude *u*, corresponding to the search space variables for the landing site. Results of Case I are discussed in detail in Chapter 4 with ground tracks and further analysis is conducted in Chapter 5.

3.2.2 Case II: Time-to-Land *T*, Right Ascension of Ascending Node Ω and Argument of Latitude *u* as Variables

The spacecraft is in some initial orbit. The exact position is unknown, but the ranges for $\bar{\zeta}$ are known**.** From some calculations and partial data obtained through the antennas, it is predicted that the spacecraft is in a circular orbit around the Moon at an altitude of 100 km above the lunar

surface. The spacecraft needs to attempt a minimum Δv_{Total} landing. For this problem, Lambert targeting by PSO is utilized to find the 10 possible landing trajectories. From Eq (2.26) and $k = 1,..7$,

$$\alpha_k = [1837.4\,km \;\; 0 \;\; 0° \;\; 0° \;\; 0° \;\; 0° \;\; 0° \;\; 0\,s]$$

$$\beta_k = [1837.4\,km \;\; 0 \;\; 180° \;\; 360° \;\; 360° \;\; 360° \;\; 360° \;\; 7000\,s]$$

This also ensures that the seven variables search space is limited within this range of $\bar{\zeta}$ during PSO. Also note that for circular orbits, θ is undefined and so in $\bar{\zeta}$, the 6th variable is *u* which is varied from 0 to 360°. For equatorial orbits where *i*, ω and Ω goes to zero, true longitude *l* is used to vary the 6th variable. Landing site coordinates are defined by latitude ϕ, longitude λ and the initial position $\bar{r}_1$ is calculated by using a, *e*, *i*, Ω, ω, θ variables contained in $\bar{\zeta}$. Initial population is randomly generated within the uniformly distributed range for each variable. Lambert calculates the Δv_{Total} after which PSO updates the values of these variables through cognitive and social information through each iteration. Each trajectory in the swarm has local best and global best values corresponding to the minimum *J* in the population through each generation. Keeping the ten best trajectories, the 90 trajectories are created using simple crossover and mutation as mentioned before. The 90 trajectories and the 10 best are the feed for the next generation. The goal of this case is to find the best J and corresponding $\bar{\zeta}$ after many generations until $J_{Optimal}$ is recorded. $J_{Optimal}$ is defined as the value of minimum J that does not change from generation to generation for 20 consecutive iterations. This enables the code to find the ten best unique combinations of the classical orbital elements and the time-to-land to reach a desired landing location on the Moon using the minimum Δv_{Total}. Chapters 4 and Chapter 5 will discuss the results, ground tracks, possible landing misses and a variety of suitable landing locations with sensitivity analysis. This case also provides a preliminary method to contemplate multiple landings on the Moon.

Chapter 4

Results

4.1 Case I Findings

This section discusses the results obtained from Case I. The section also outlines various optimal cost functions calculated corresponding to different landing sites after 100 generations.

Various combinations of λ and ϕ in the first quadrant ranges are simulated for multiple cases of Lambert targeting and PSO code generated in MATLAB. More information on the coding procedures is presented in the Appendix. Generating 100 initial trajectories with different T values calculated J, which ranged from 2.92 km/s to 20 km/s for the selected landing site. The ten best trajectories that have a minimum J for each generation were plotted and carried through the generations until $J_{Optimal}$ was calculated and produced new best trajectories with suitable T. Table 4.1 includes some landing sites to their corresponding cost functions and the time-to-land T. Most of the landing sites presented in table 4.1 uses the initial conditions for a perfectly circular orbit at an altitude of 100 km with inclination 0°, unless otherwise mentioned. The values of other Euler angles, Ω and ω are also taken as 0°. The value of argument of latitude is denoted as 0° for a starting position defined in Case I for results presented in Table 4.1.

It was observed that the value of J, cost function increased as the value of λ and ϕ increased and the calculated time to land T also increased and adopted a wider range. This can be evident from the values of T in Table 4.1 for the landing locations at or near the poles. At the landing site of λ=0° and ϕ=0°, at the equator, the value of J remained lower for equatorial orbit at i=0° and increased as inclination increased. This makes sense in terms of plane change maneuvers as well, where larger inclination changes between orbits requires larger Δv_{Total}. The selected landing site of ϕ=0° and λ=0°, is near the "Hipparchus" crater on the Moon precisely at the "Sinus Medii" crater at the center of the visible Moon's surface[28]. Another landing site with coordinates ϕ=30° and λ=0°,

is presented in Table. 4.2 which is just a few degrees away from the Apollo 15 landing site Hadley/Apennines at ϕ=26.13222° and λ=3.63386° and the calculated distance[23] is 301 nautical miles or 558 km[22]. To mark the 50th Anniversary of the first man landing on the Moon, Apollo 11 landing site, "Mare Tranquillitatis" crater was is investigated for PSO optimization through Lambert's solution. The value of $J_{Optimal}$ and time to land, corresponding to the Apollo 11 landing site are presented in Table 4.1.

Table 4.1: Optimal data for Case I using different landing sites

Latitude	Longitude	J at generation 1	$J_{Optimal}$	T
Degree (N)	Degree (E)	(km/s)	(km/s)	s
0	0 E	1.724	1.721	3399.0
0	0 (i = 10°)	1.983	1.982	3397.8
0	0 (i = 20°)	1.729	1.722	2487.9
0	0 (i = 45°)	2.949	2.940	3393.4
90	0 (i = 10°)	3.917	3.916	6840.6
30	0	3.948	3.936	6991.2
0.06741	23.47297	1.746	1.744	6947.3

4.1.1 Investigating Landing site of ϕ=0° and λ=0°

According to the values presented in Table 4.1 and the corresponding ground tracks presented later in this section, the evolution of trajectories over several generations is recorded. The results presented in this thesis start from many initial conditions, constraints, and assumptions mentioned earlier in Chapters 2 and 3. To be concise, some of the initial conditions used for the simulation of Case I, to land at the "Sinus Medii" crater, are presented in Table 4.2. Sensitivity of the initial conditions used is presented in Chapter 5. In Case I, only *T* is the search space variable for PSO optimization, and the limits of *T* are decided based on the Kepler's third law of motion that relates period of an orbit to its semi-major axis a.

Table 4.2: Initial conditions for Case I for λ=0° and ϕ=0°

Variable	Value
Altitude (fixed)	100 km
Eccentricity *e* (fixed)	0
Inclination *i* (fixed)	20°
Right ascension of ascending node **Ω** (fixed)	0°
Argument of periapsis ω (fixed)	0°
Argument of latitude *u* (fixed)	50°
T (Variable)	0 -7000 s

Figure. 4.1 illustrates the behavior of an initial pool of 100 trajectories which is used to find the ten minimum Δv_{Total} for that population and then a new set of the population is generated using the dependency (mutation and crossover) from the previous generation's fitness values. Figure. 4.2 introduces the behavior of the swarm after 100 generations of Lambert targeting using PSO. The minimum Δv_{Total} for the entire swarm is 1.7293 km/s in Fig. 4.1 and is 1.7229 km/s in Fig. 4.2, marked with a star marker. As illustrated in the graphs, cost function or Δv_{Total} is scattered and sometimes showed larger values such as 50 km/s at the initial population after which the range of distribution gets smaller through generations and ends up between 0 km/s to 10 km/s in Fig. 4.2. This does not affect the 10 best trajectories that are sorted at the end of each generation but affects the population convergence for sure. This can also be referred to the inertial coefficient, cognitive coefficient and the social coefficient from Eq. (2.26) in Chapter 2. Cognitive coefficient takes in account the local best values while the social coefficient takes in account global best values throughout the population and through the generations. Therefore, using wide ranges for the decision variables might affect the convergence.

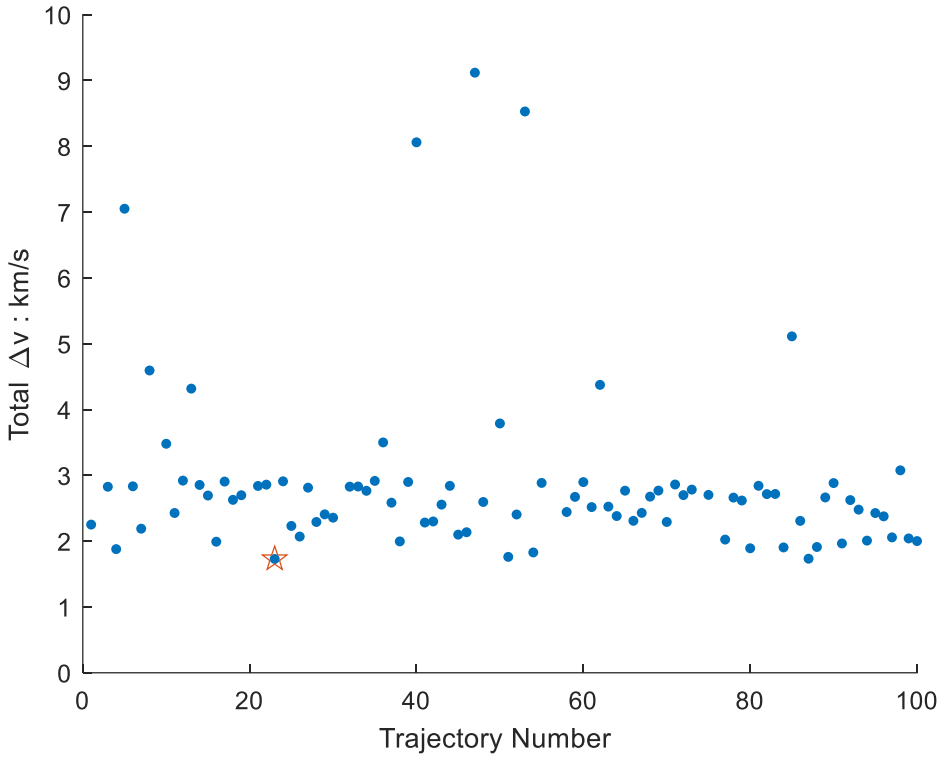

Figure 4.1: Cost function for the Initial Population in Case I generated stochastically.

As mentioned in Case I definition and table 4.2, the initial population starts with a perfectly circular orbit at an altitude of 100 km above the surface of the Moon inclined at 20° from the equatorial plane of the MCI coordinate system. The only search variable, in this case, is T and hence most of the data in this section elaborates on T. Further analysis in Chapter 5 throws more insights into the importance of the classical orbital elements and the initial conditions.

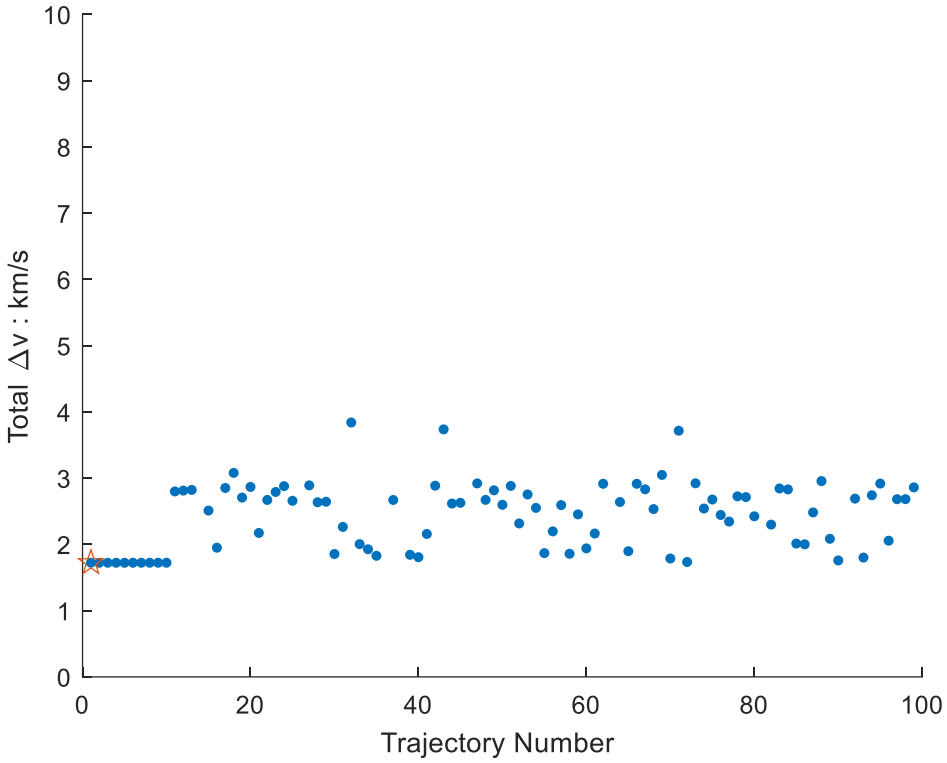

Figure 4.2: Cost function for the 100th population after optimization.

Figure 4.3 identified the Δv_{Total} values of the ten best trajectories in each generation. As expected, values of consecutive ten trajectories are spread apart and start at some initial Δv_{Total} in km/s which are then carried through generations with new better or lower Δv_{Total} values in km/s. Different colored points are used to differentiate the 10 best Δv_{Total} of one generation from another. At each generation in Fig. 4.3, ten same colored points represent the 10 best Δv_{Total} after which the color changes for the 10 best Δv_{Total} of the next generation. After around 50 generations, the ten points per generation, superimpose on each other to indicate convergence. Finally, the difference between the ten consecutive Δv_{Total} and the minimum Δv_{Total} from the previous

generation, gets less than 10^{-3} to mark convergence. The horizontal axis of Fig. 4.3 is reduced for better visualization of the progression of the cost function. Depending on the initial conditions used, the convergence can occur at an earlier generation or at a later generation. Most of the iterations tested for this Case converged between 50 to 300 generations and so the maximum number of iterations chosen for the analysis presented in this section is 100. Large number of generations were also used to record the changes in Δv_{Total} corresponding to the values of T obtained, for various combination of initial conditions used for that case. This is discussed more in detail in the sensitivity analysis portion of Chapter 5.

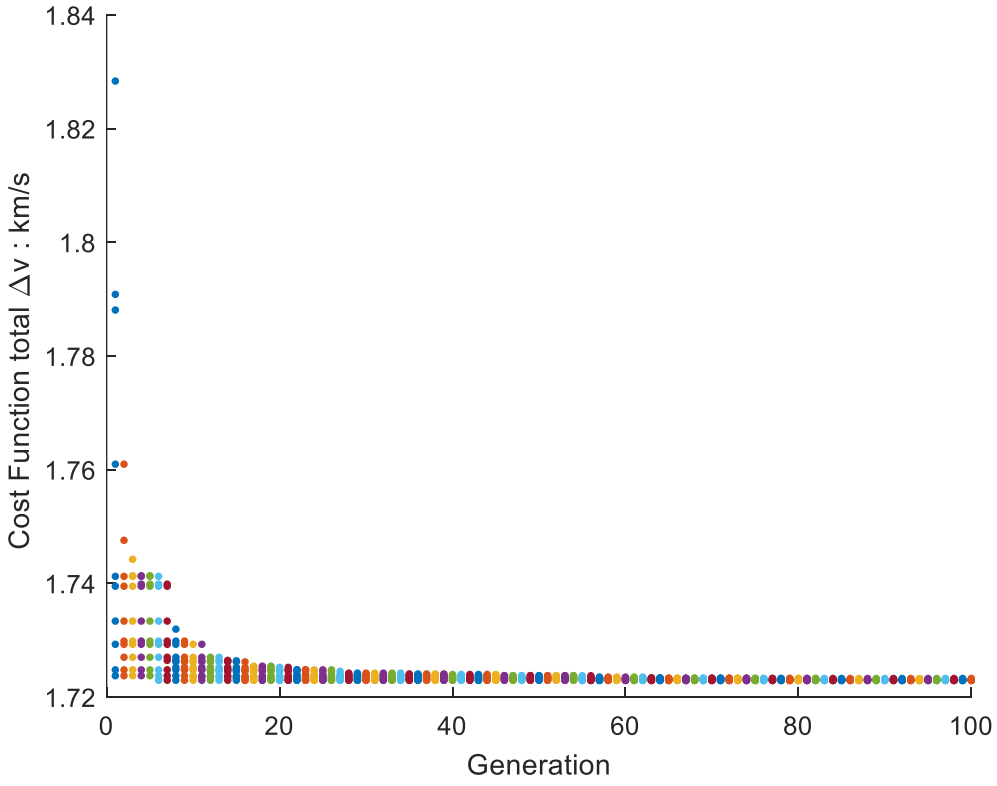

Figure 4.3: Progression of the ten best cost function J over generation of trajectories.

Figure 4.4 shows the cost function, J in km/s, through the generations. It follows a normal Pareto frontier pattern to indicate convergence. Similar graphs were produced for other landing

sites through the simulations. The $J_{Optimal}$ for such cases were lower for landing sites near the equator and near prime meridian/zero longitude on the Moon and increased moving closer to the poles. Not only, in $J_{Optimal}$ but there is a difference in time-to-land T, moving away from the equator. Larger T was observed for landing sites after ϕ=50° and λ=50° and lower T was discovered near ϕ=0° and λ<=30°. For landing at the North pole or the South pole from the initial equatorial circular orbit, large $J_{Optimal}$ of 3.91 km/s was recorded which demands more propellant usage and other plane change maneuvers.

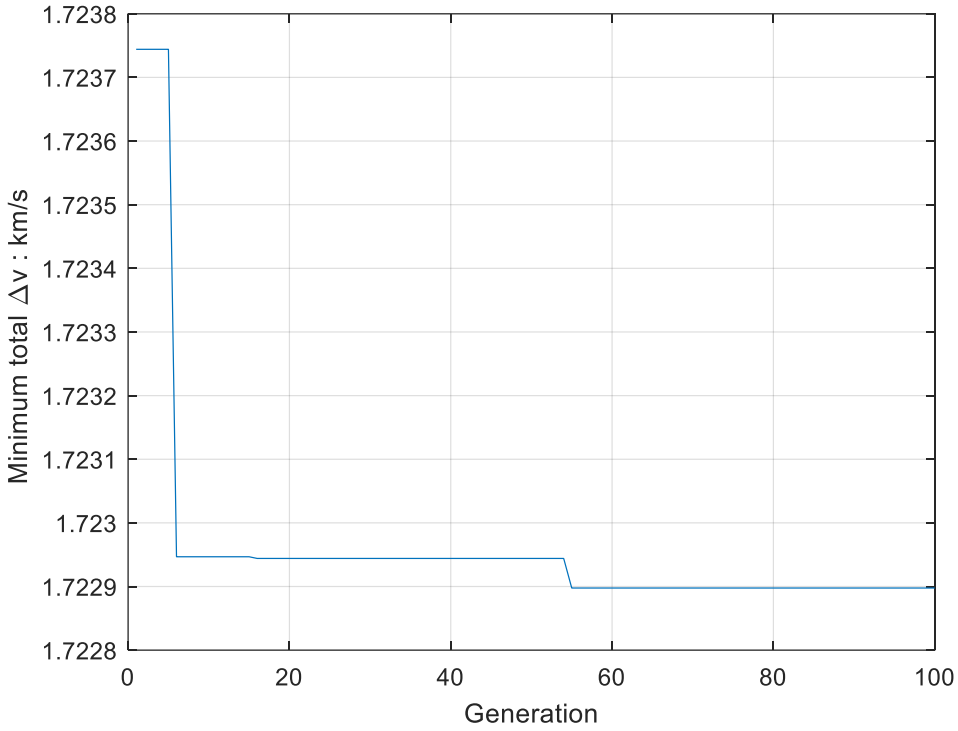

Figure 4.4: Optimal J for a landing site of ϕ=0° and λ=0° in Case I

Figure 4.5 illustrates the ground track of a spacecraft to land on the lunar surface. As mentioned before, a landing site was selected at the beginning of this optimization process and results for ϕ=0° and λ=0° for Case I are included in Fig. 4.5. The ground tracks passed through the same latitude and longitude as the landing site. With the 10 trajectories selected at the end of the PSO process, multiple landing attempts can be made, thereby reducing the landing ellipse by further

analysis. Ground tracks for this analysis, are created using the ode45 feature of MATLAB that integrates the initial state vector consisting of $\bar{r}_1$ and $\bar{v}_{1lambert}$ for Case I through the time-to-land T for the selected landing site. The equations of motion[15] used are the simple two body equations. The final state vector after integration is converted into the topocentric coordinate system or the latitude and longitude which is then used to generate graphs like Fig. 4.5 and Fig 4.10. Figure 4.5 depicts the Mercator projection of the Moon map[28], developed for NASA by the U.S. Geological Survey. This map starts from -90° west longitude on the Earth's visible side of the Moon and ends at 90° to the East. According to Fig. 4.5, for starting at a circular orbit at the far side of the Moon, the lander reaches at the "Sinus Medii" crater at ϕ = 0° and λ = 0°. Ground track of the lander is marked in yellow while the start and finish points are marked in red. The descent point P_1 coordinates are ϕ = 15.19° and λ = -132.14°, between "Poynting" and "Fersman" craters on the far side of the Moon.

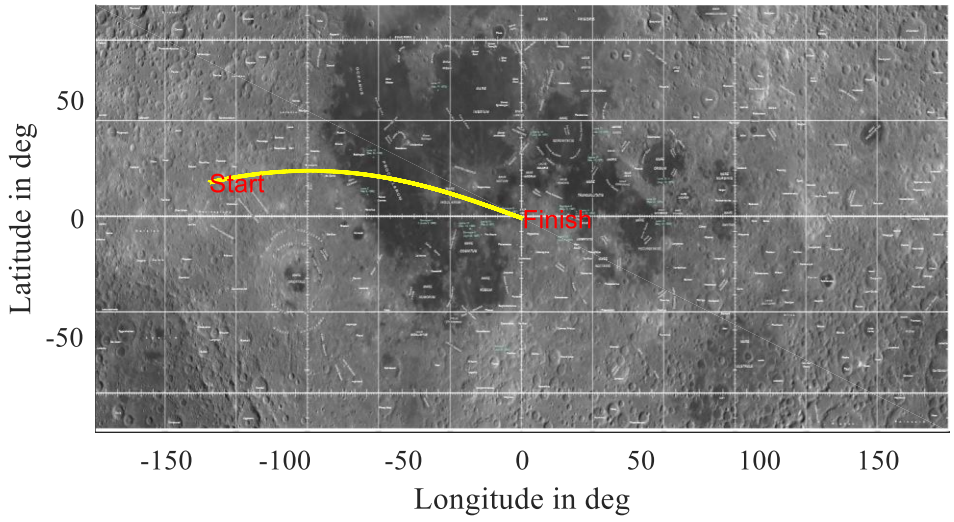

Figure 4.5: Ground track for a landing site of ϕ=0° and λ=0° in Case I.

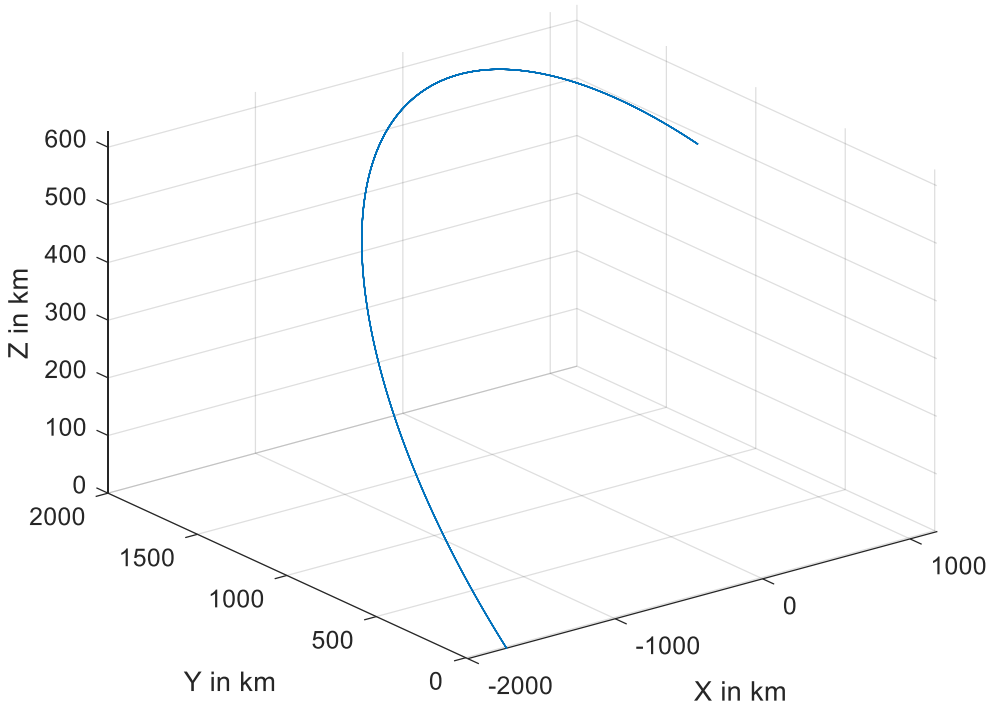

Figure 4.6: Trajectory at $J_{Optimal}$ for a landing site of ϕ=0° and λ=0° in Case I.

Literature also provides some stability analysis on some longer period repeatable lunar groundtracks which also takes into account, the perturbation effects due to the Earth and the sun.[19] Fig. 4.7 compares the altitude of the spacecraft to its downrange and indicates landing after 2487.9 s through altitude progression with time data in Fig. 4.8. It is to be noted that the ground track in Fig. 4.5 takes into account the rotation of the Moon with respect to the east longitude.

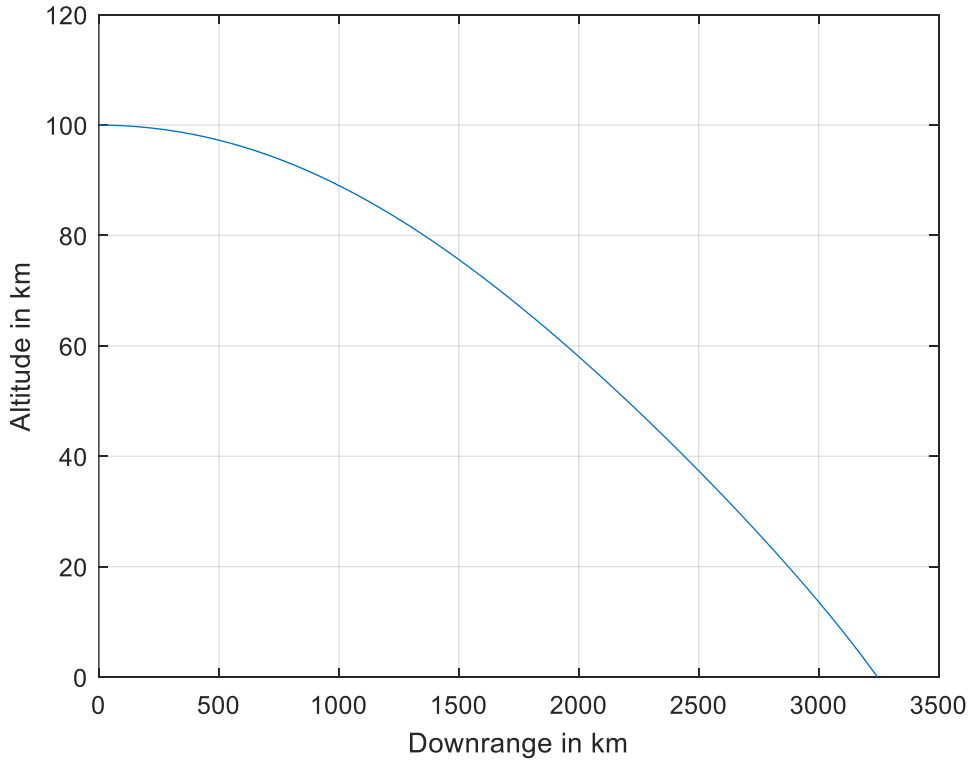

Figure 4.7: Altitude versus downrange at $J_{Optimal}$ for a landing site of ϕ=0° and λ=0°.

To better understand the satellite tracking data the downrange, altitude and cross-range have been used in radar basics. Downrange is defined as the horizontal distance between the spacecraft and the descent point P_1 during the transfer. As evident from Fig. 4.7 and Fig 4.9, downrange increased as the altitude decreased, and time-of-flight increased, reaching a maximum downrange at landing. Altitude starts at 100 km and reaches 0 km altitude in 2487.9 seconds (41.46 minutes). The time-to-land for the other 9 trajectories with minimum J also recorded T around this value. Downrange reached 3226 km at landing time as depicted in Fig. 4.9.

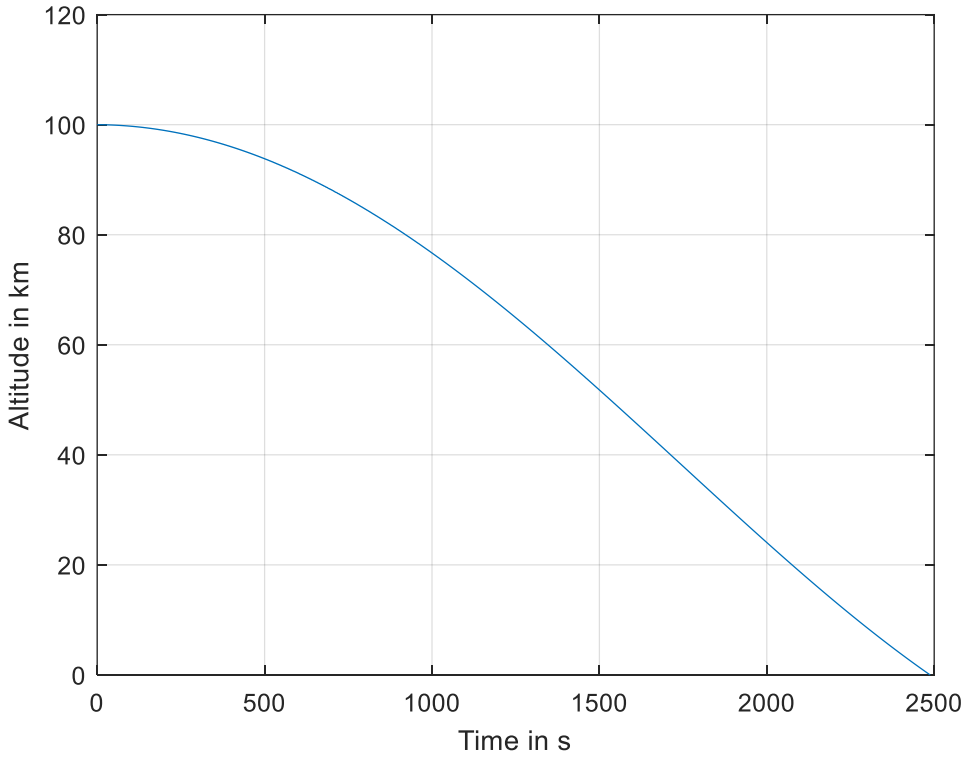

Figure 4.8: Altitude versus time at $J_{Optimal}$ for a landing site of ϕ=0° and λ=0°.

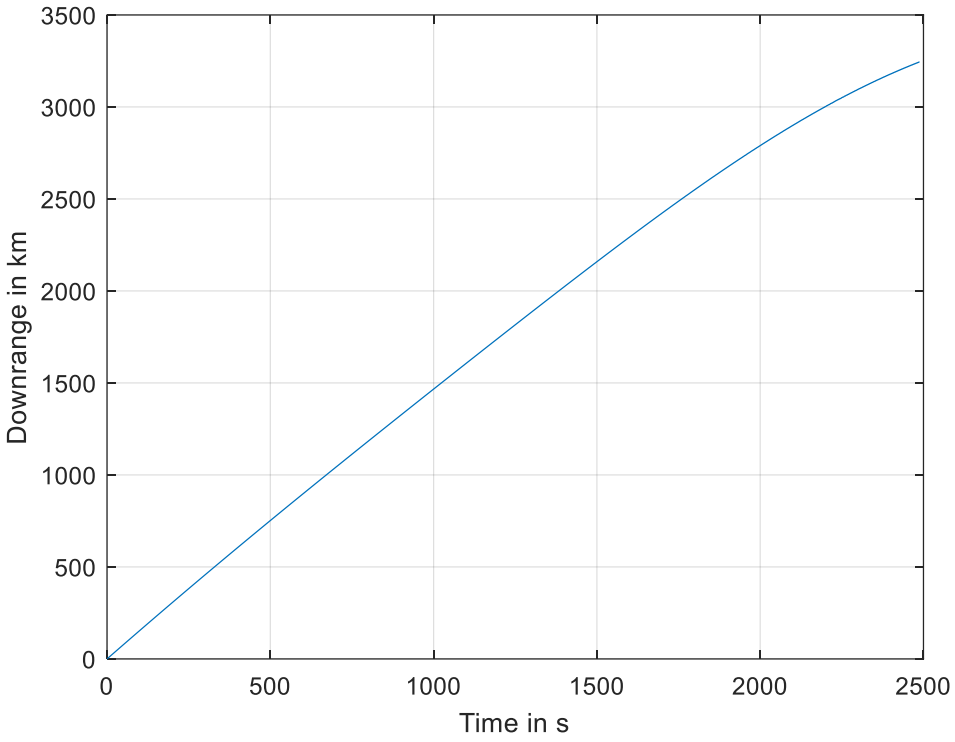

Figure 4.9: Downrange versus time at $J_{Optimal}$ for a landing site of ϕ=0° and λ=0°.

Results presented in this section used the case of only circular orbits. Additional details on the starting position of the spacecraft and the orientation of the transfer plane with respect to the equatorial plane is discussed in Chapter 5.

4.2 Case II findings

For a better analysis of the results and comparison with Case I, the selected landing site for this case is ϕ=0° and λ=0°. Figure 4.10 demonstrates the swarm behavior at the initial population that contained randomly distributed values of, Ω, u and T between ranges [0° 360°], [0° 360°] and [0 7000] s consecutively. This Case keeps the values of a, e and i constant for a better analysis of results for various trajectory transfer plane orientations. It also considers special cases of equatorial circular orbits or perfectly circular orbits, where some of the variables in $\bar{\zeta}$ are undefined when u and l are introduced. After solving for Lamberts solution of calculating required velocities to reach point P_2 from P_1, PSO algorithm specified in Chapter 2 is applied which then sorts 10 trajectories having the minimum J in the swarm. This minimum J, when compared through several iterations, $J_{Optimal}$ is found.

4.2.1 Investigating Landing site of ϕ=0° and λ=0°

This section includes results for a spacecraft at 100 km altitude around the surface of the Moon with a circular trajectory inclined at 10° to the MCI equatorial plane while attempting to land at the site of ϕ=0° and λ=0° for Case II. The initial conditions used for the data presented in this section are included in Table 4.3 and the search space variables are highlighted in pink. Figure 4.11 demonstrates the progression of the swarm behavior after 5000 generations. The reason for having a large number of generations for this Case is that larger search space is introduced compared to Case I and stability of search space variables corresponding to J increased at larger generations leading to $J_{Optimal}$.

Table 4.3: Initial conditions for Case II for λ=0° and ϕ=0°

Variable	Value
Altitude (fixed)	100 km
Eccentricity *e* (fixed)	0
Inclination *i* (fixed)	10°
Right ascension of ascending node Ω (variable)	0° – 360°
Argument of periapsis ω (fixed)	0° – 360°
Argument of latitude *u* (variable)	0° – 360°
T (variable)	0 -7000 s

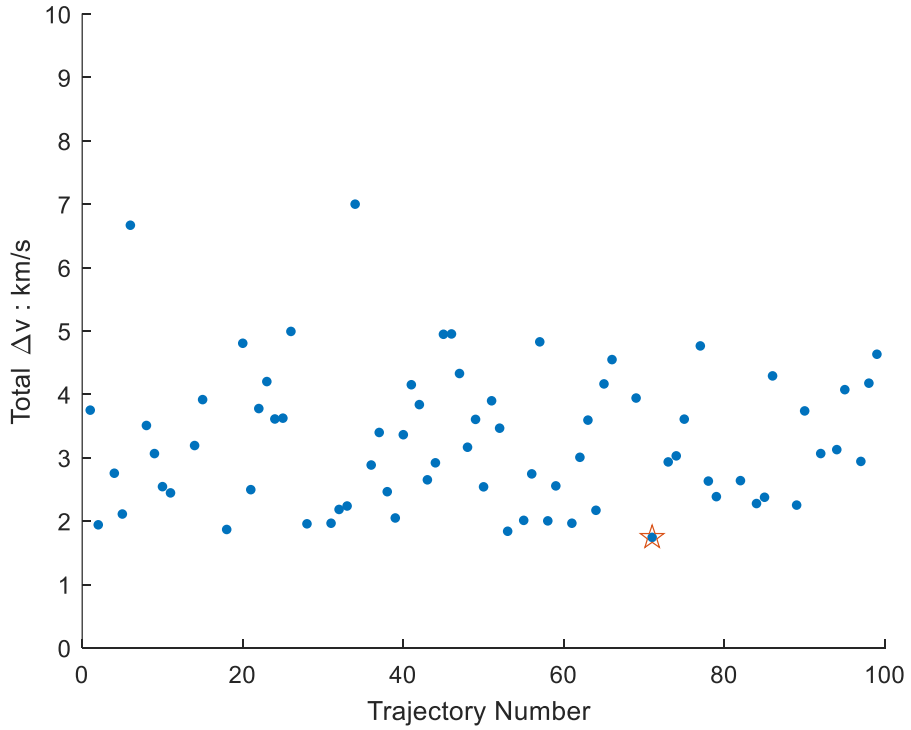

Figure 4.10: Cost function for the Initial Population in Case II generated stochastically.

After introducing different number of iterations to confirm the convergence and to record the changes in cost function J, it was observed that some values of classical orbital element variables also followed repetition with the cost function. Figure 4.10 presents the swarm behavior in terms of cost function J at the initial population generation. This population have not yet encountered PSO and is randomly generated as mentioned in Chapter 3. The spread of Δv_{Total} is reduced significantly in Fig 4.11, from Fig 4.10 which is the essence of swarm optimization. Local best J is marked in a red star which is 1.743 km/s in Fig. 4.10 at the initial population, reduced to 1.722 km/s in Fig. 4.11. Large values of Δv_{Total} were also recorded for some hyperbolic trajectories in a swarm indicating the flexibility of this algorithm to search for other possible conic sections and prune it according to the requirements. However, for this analysis, only circular trajectories are presented.

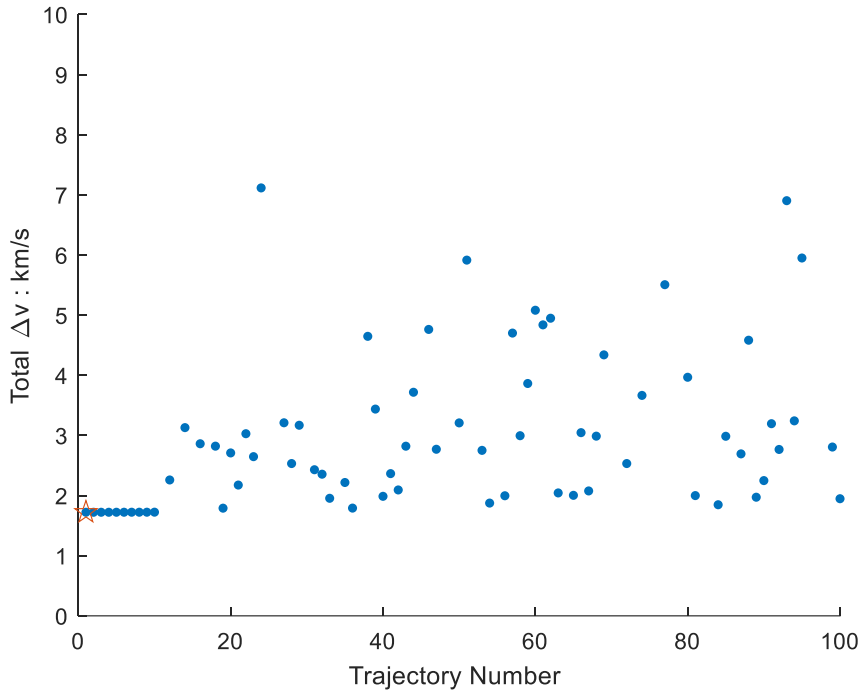

Figure 4.11: Cost function for the 5000th population in Case II after optimization.

The analysis conducted for this thesis relies heavily on the Pareto frontier like graph presented in Fig. 4.12 and Fig 4.13. Figure 4.13 provided evidence that $J_{Optimal}$ for the trajectory converged to 1.72215 km/s after about 2000 generations for different conditions in Case II. Note that $J_{Optimal}$ is the minimum Δv_{Total} for the entire swarm which also translates to the minimum Δv_{Total} among the 10 best selected trajectories at each generation. The definition of convergence for this thesis is that $J_{Optimal}$ should stop changing by tolerance not less than 10^{-3} km/s, generation after generation and that definition is supported by the results in Fig. 4.12. As mentioned before, the single colored 10 points at each generation represent the ten minimum Δv_{Total} at that generation. The horizontal axis of Fig. 4.12 is reduced from 5000 generations to 100 generations for clarity in visualization and analysis.

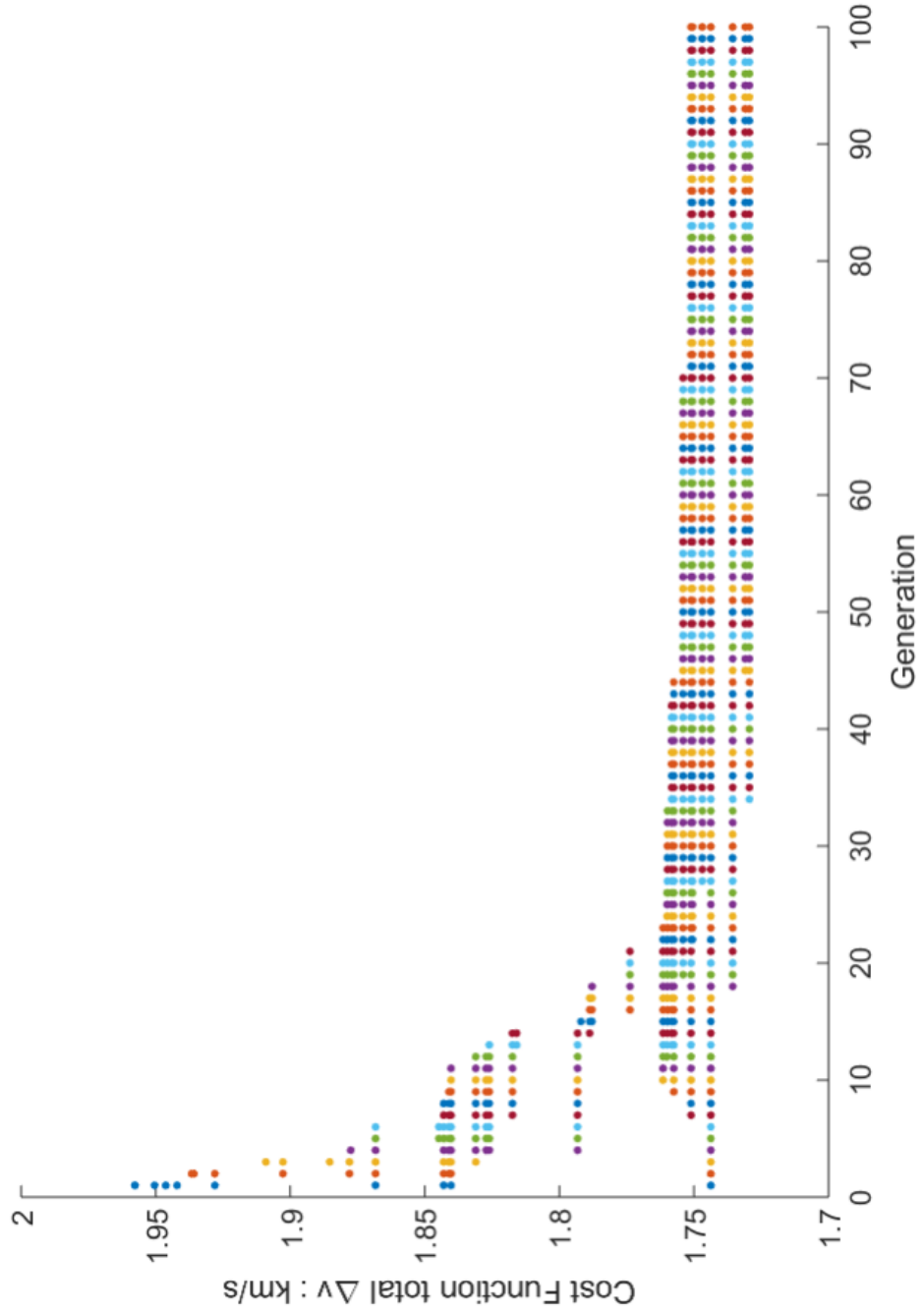

Figure 4.12: Progression of the ten best cost function J over generation of trajectories.

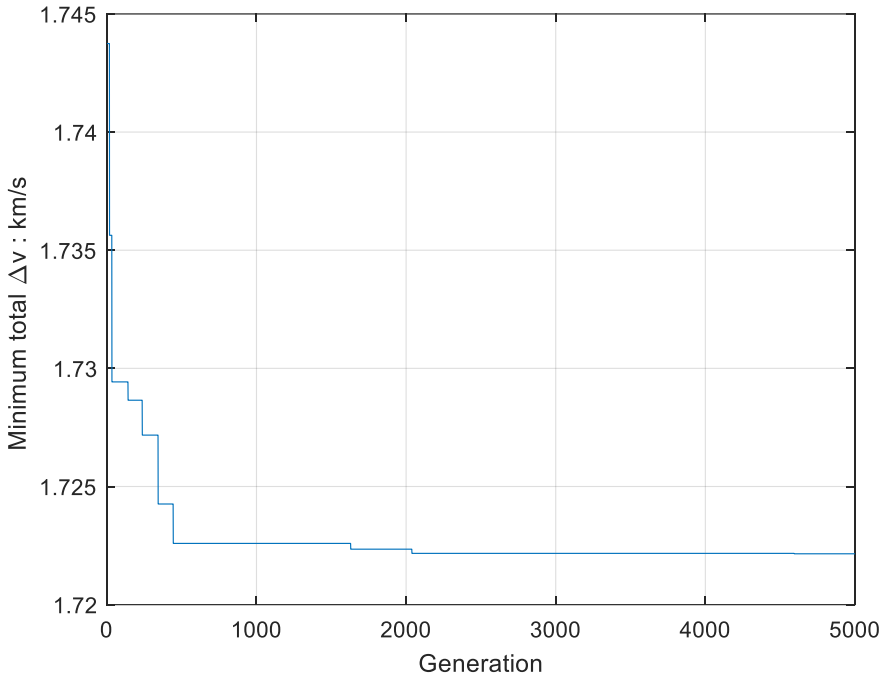

Figure 4.13: Optimal J for a landing site of ϕ=0° and λ=0° in Case II.

Data presented in Table 4.4 are trajectory characteristics in the form of classical orbital elements at the end of 5000 generations at the "Sinus Medii" landing site. Through PSO, a unique combination of classical orbital elements to satisfy our minimum cost function requirements is presented in Table 4.4. Initially, a random population is generated that falls under a specified uniformly distributed range described in detail in Chapter 3, then crossover and mutation are involved to generate the new population for the next iteration to ensure dependence between generations. This process leads to some "sweet" spots or ranges that can be considered for a mission to attempt multiple landings. Calculated values of J ranged from 1.722 km/s to 2.05 km/s with a unique combination of the classical orbital elements and the time to land during the search process.

Table 4.4. 10 best trajectories with unique $\bar{\zeta}$ and cost function J

	a	i	Ω	u	T	J
	km	degrees	degrees	degrees	s	km/s
1	1837.4	10	0.47	35.56	2746.7	1.72
2	1837.4	10	0.83	343.5	6184.2	1.72
3	1837.4	10	0.45	308.3	3956.6	1.72
4	1837.4	10	0.68	15.67	3100.9	1.72
5	1837.4	10	180.87	204.25	2945.6	1.72
6	1837.4	10	181.02	132.3	6840.9	1.72
7	1837.4	10	0.98	63.53	2214.4	1.72
8	1837.4	10	180.85	216.60	2730.7	1.72
9	1837.4	10	179.84	250.64	2101.8	1.72
10	1837.4	10	180.61	223.77	2607.6	1.72

Analogous to Case I, a ground track was generated for the trajectory that has the minimum J and that is $J_{Optimal}$ for that case. With reference to Table 4.4, trajectory 1 at a circular orbit of 100 km altitude, inclined at 10°, with its ascending node located at 0.47° from the point of Aries and at 35.56° angular distance from the equatorial plane of the Moon follows a curve illustrated in Fig. 4.14. This curve plots the position of the lander throughout time-to-land in MCI frame.

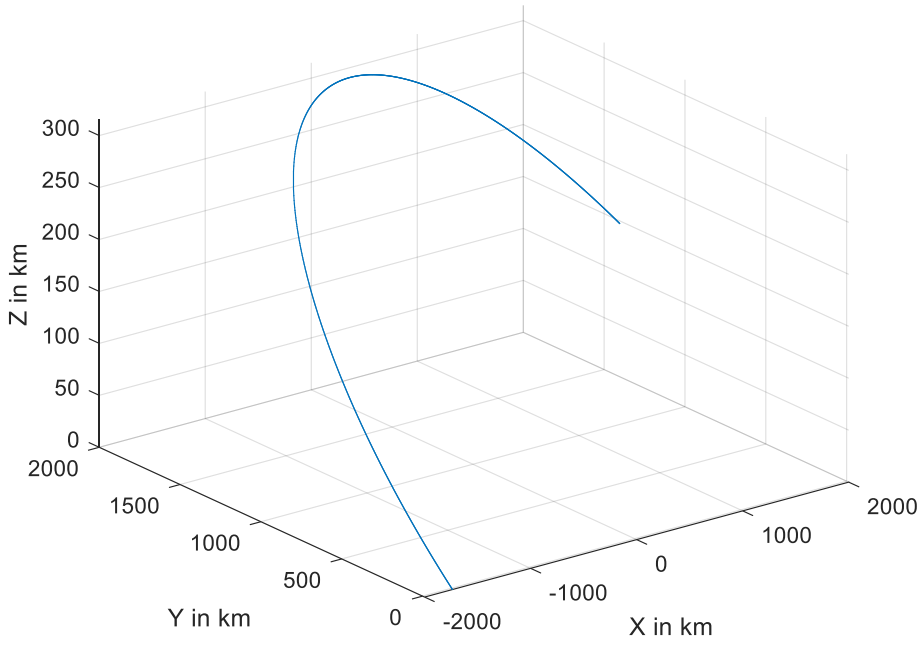

Figure 4.14: Trajectory at $J_{Optimal}$ for a landing site of ϕ=0° and λ=0° in Case II.

Figure 4.15 is the ground track of the lander which starts at a latitude of ϕ = 5.79° and longitude of λ = -144.8°. Note that -144.8° longitude corresponds to the west longitude and is located at the far side of the Moon near "Tsander" crater. Terrain features can drastically affect landings and so, while selecting landing sites for each case in Chapter 4 and Chapter 5, some of the topographical surfaces are considered. Thus, latitudes and longitudes of the landing site near deep craters or a group of small craters are avoided.

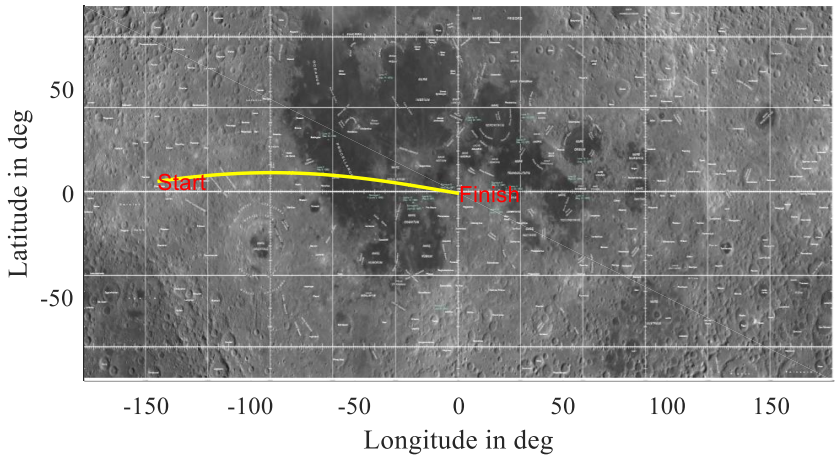

Figure 4.15: Ground track for a landing site of ϕ=0° and λ=0° in Case II.

Figure 4.16 presents the progression of altitude with respect to downrange for the selected landing site and it reached 3391 km downrange at landing. It is also evident from Fig. 4.17 and Fig. 4.18 that the altitude reached 0 km with respect to the ground around 2747 seconds. This is also supported by downrange progression with time data in Fig. 4.18.

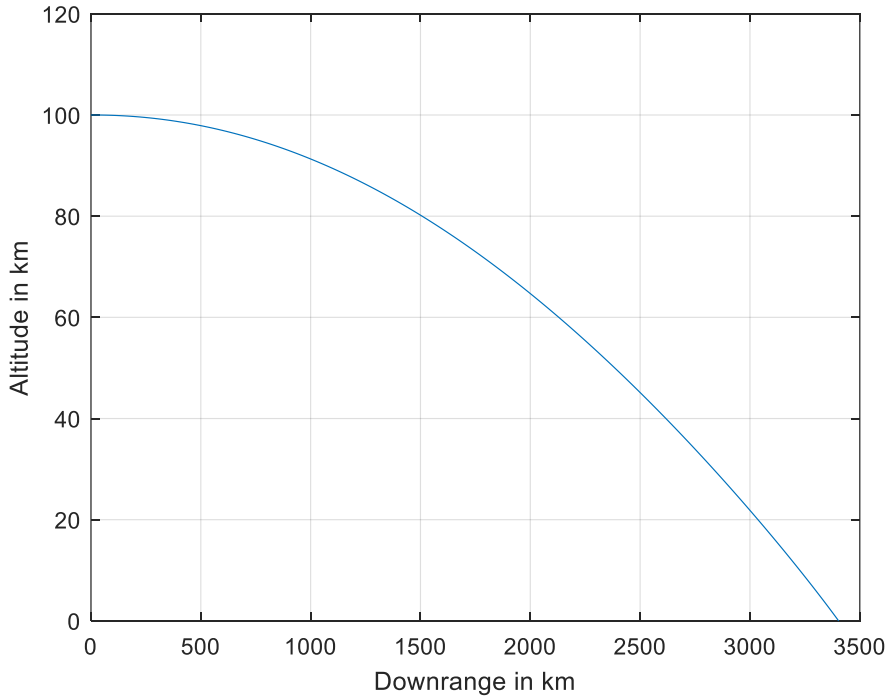

Figure 4.16: Altitude versus downrange at $J_{Optimal}$ for a landing site of ϕ=0° and λ=0°.

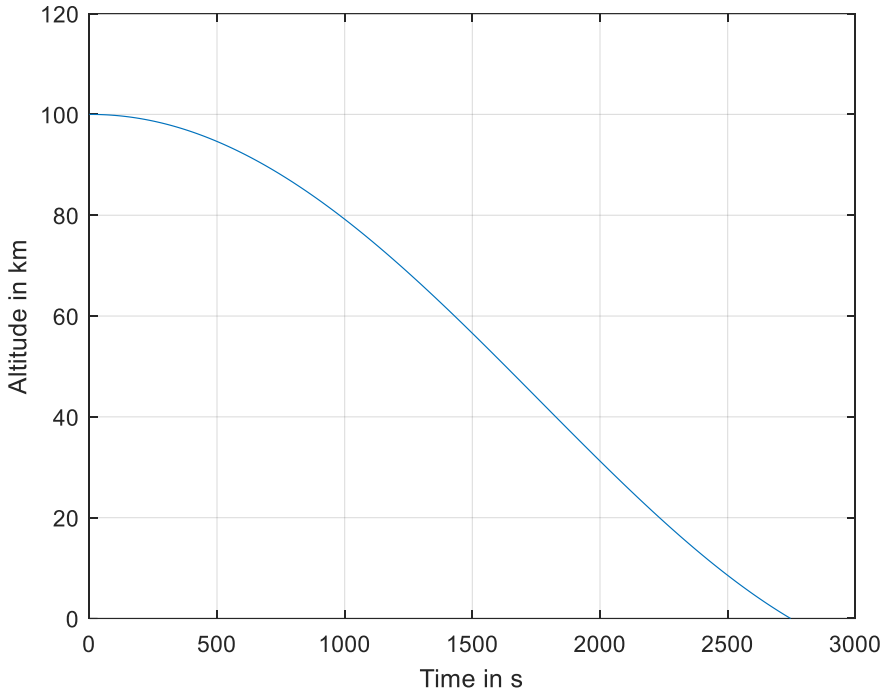

Figure 4.17: Altitude versus time at $J_{Optimal}$ for a landing site of ϕ=0° and λ=0°.

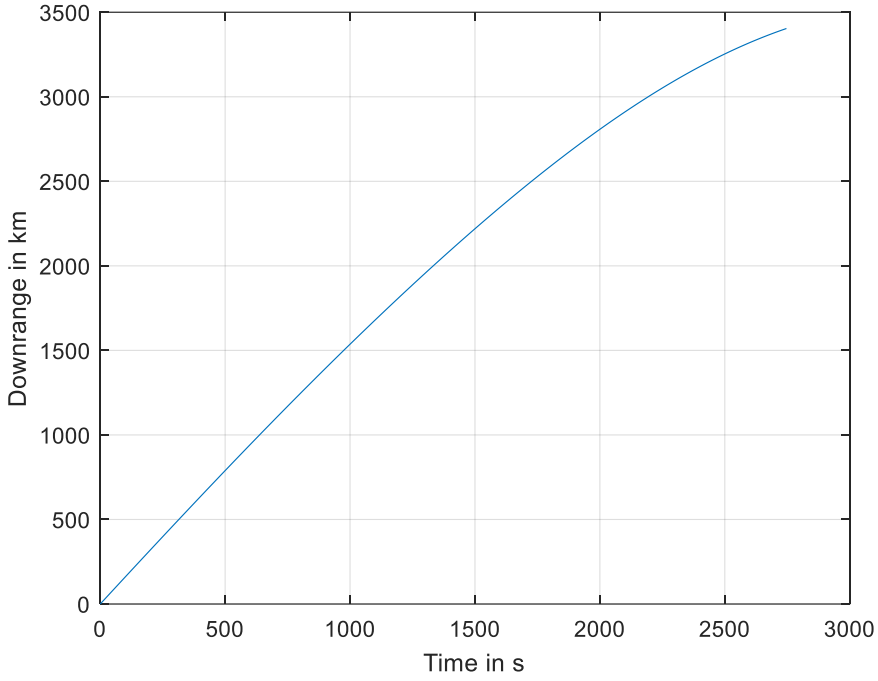

Figure 4.18: Downrange versus time at $J_{Optimal}$ for a landing site of ϕ=0° and λ=0°.

Figure 4.19 generates the ground track of the ten trajectories included in Table 4.4. A unique combination of the classical orbital elements and the time-to-land for each of these ten trajectories was used to integrate the initial position, obtained from classical orbital elements, through a time of flight to produce ground tracks illustrated in Fig. 4.19. All the 10 trajectories pass through the selected landing site "Sinus Medii" and provides support to the results in Table 4.4 and the overall analysis. Note that the ground track of trajectories 2 and 6 are not included to increase the readability of Fig. 4.19, while comparing the 10 best trajectories. The values of time-to-land for trajectories 2 and 6 in Table 4.4, is closer to the period of the initial orbit (7066 s) and the ground track is similar to trajectory 3 in Fig. 4.19.The starting latitudes and longitudes for each trajectory in Fig. 4.19, are presented in Table 4.5. As evident from Table 4.5, the starting coordinates for the descent are in the South-West region of the Moon map. The analysis presented in this section and from Case I have minute differences in the $J_{Optimal}$ values for similar conditions considered. Case

I only searched for $J_{Optimal}$ based on T while Case II reached $J_{Optimal}$ by searching through the three variables. This points to the importance of strong identification of first attempt solution or constraints that lead to optimization. T improved in Case II for various landing sites with the same initial conditions. Inclination played a role in finding lower $J_{Optimal}$ corresponding to the landing site coordinates. Higher $J_{Optimal}$ was recorded for the poles with no inclination and lower $J_{Optimal}$ for inclination closer to the latitude of the poles. This was also observed at the equator. In Case I, lower $J_{Optimal}$ of 1.7294 km/s was calculated for equatorial orbit while greater $J_{Optimal}$ of 1.982643 at i=10° was recorded. This provides insight into the sensitivity of the classical orbital element variables used in the optimization process as well as the choice of landing site coordinates which is presented in Chapter 5.

Table 4.5. Latitudes and Longitudes of the starting point for the best trajectories in Case II

Trajectory	ϕ (degree)	λ (degree)
1	5.79° N	144.8° W
3	7.83° S	128.57° E
4	2.68° N	164.34° W
5	4.09° S	155.66° W
7	8.94° N	166.18° W
8	5.94° S	143.38° W
9	9.42° S	110.12° W
10	6.98° S	136.45° W

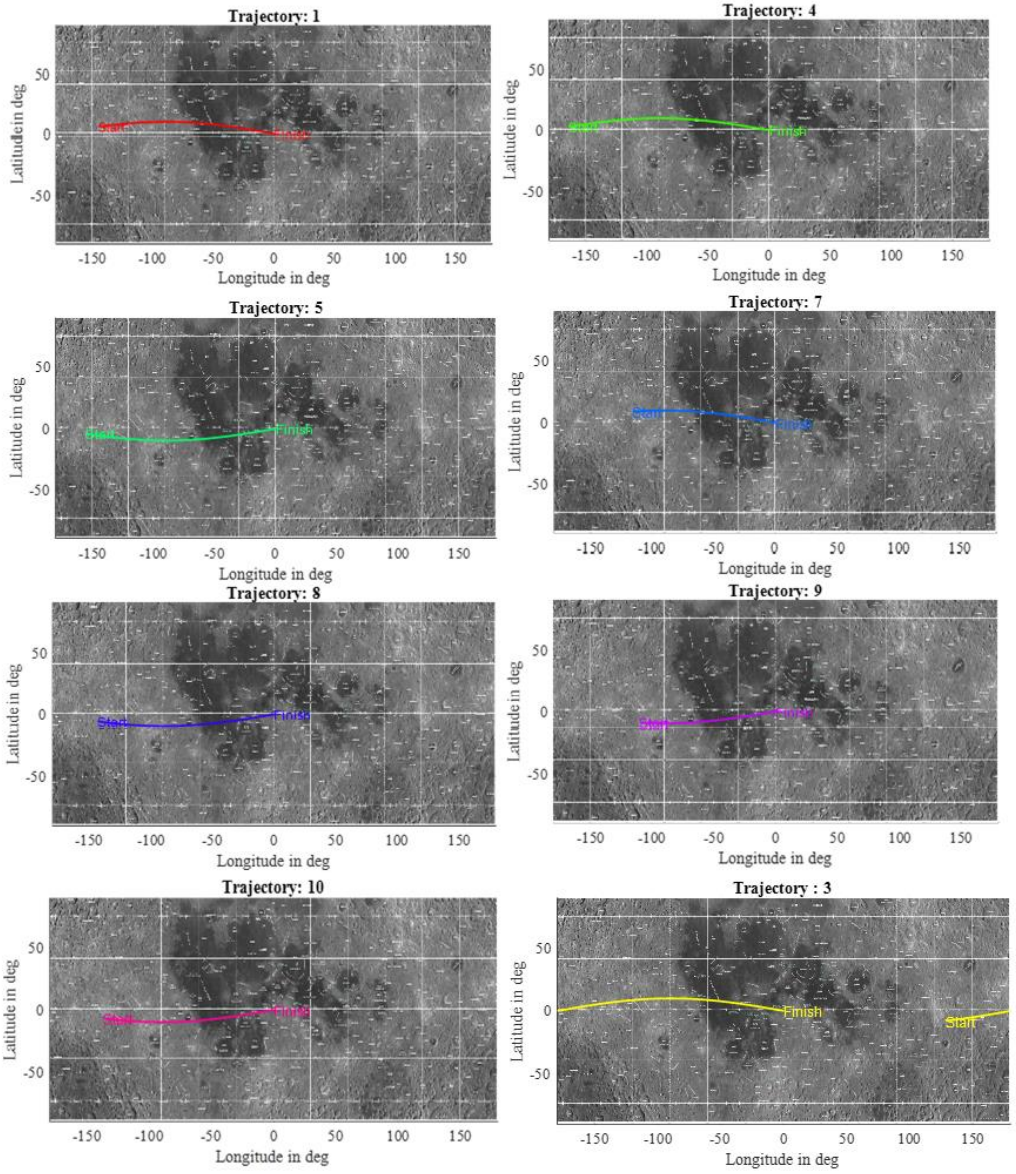

Figure 4.19: Ground track for the other trajectories from Table 4.4 in Case II.

Chapter 5

Sensitivity Analysis

Chapter 4 presented the results for these two cases and seems to find an optimal landing trajectory with appropriate optimized attributes. This section will elaborate on the details that lead to such predictions and observations. As mentioned before, increased number of assumptions for an astrodynamics problem might be disadvantageous and can affect spacecraft negatively and can lose its trajectory for a long period. Throughout this section, variables in $\bar{\zeta}_i^1$ for Case I as well as Case II will be examined for interdependency on results and the overall process of PSO.

5.1 Classical Orbital Elements

5.1.1 Inclination of the orbit

Using the value of $\bar{\zeta}_i^1$ as indicated in Case I affected $J_{Optimal}$ with changes in inclination as well as changing initial conditions from perfectly circular, non inclined orbits to other values for classical orbital elements' Euler angles. Figure 5.1 indicates the $J_{Optimal}$ values for various inclination angles over generations for Case I. It was predicted that $J_{Optimal}$ will be lower for inclination closer to 0° and would be greater for higher inclined orbits and that is supported by Fig. 5.1. In Fig. 5.1, ideal behavior is noticed for prograde orbits where $J_{Optimal}$ is low for small inclination orbits and gets larger for highly inclined orbits. It is to be noted that the initial conditions used for Fig. 5.1 does not correspond to the values presented in Table 4.2 and used 0° for the right ascension of ascending node Ω, the argument of periapsis ω and the true anomaly θ for a landing site at the "Sinus Medii" from Chapter 4.

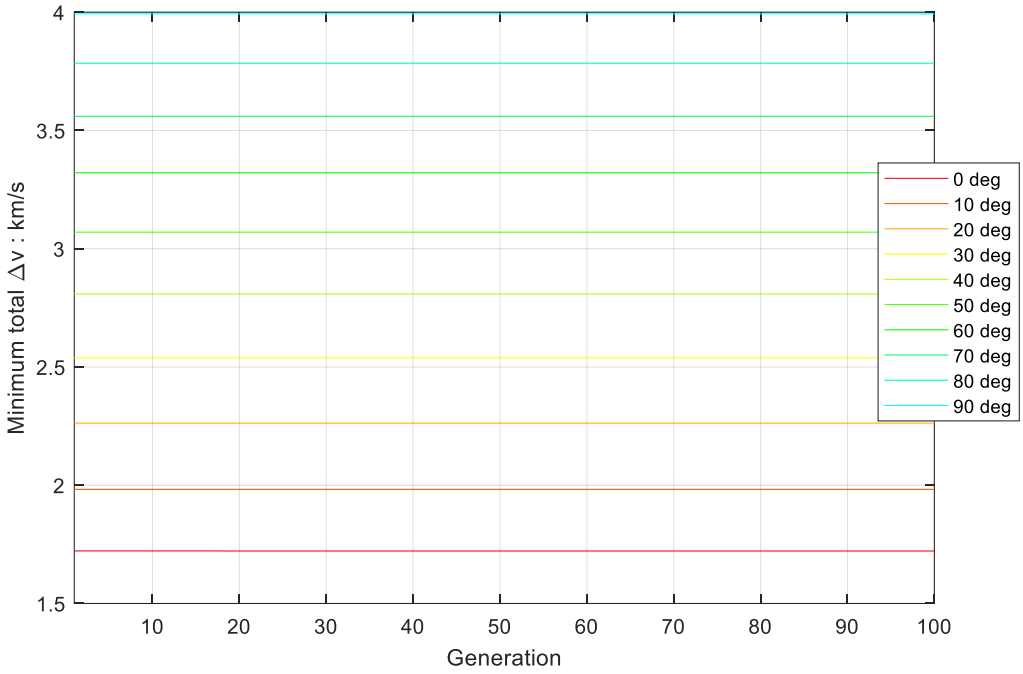

Figure 5.1: Sensitivity through a change in inclination for a landing site of $\phi=0^0$ and $\lambda=0^0$

Results for the initial conditions presented in Table 4.2 for Case I are used to investigate a change in $J_{Optimal}$ values for inclination changes, illustrated in Fig 5.2. Figure 5.2 uses conditions for prograde orbits starting at a circular orbit at an altitude of 100 km above the surface of the Moon. The results in Fig. 5.2 also align with the results in Fig. 5.1 in terms of pattern. At lower inclination, lower $J_{Optimal}$ was recorded, while at higher inclinations, larger $J_{Optimal}$ or Δv_{Total} was required for landing. Similar behavior was recorded for retrogade orbits but it did not follow the accurate pattern from Fig 5.1 and Fig 5.2. Retrogade orbits follow a direction opposite to the rotation of the Moon. Therefore, as evident from Fig. 5.3, lower Δv_{Total} is needed for highly inclined orbit such as 180° and larger Δv_{Total} for 120°. Note that orbit at inclination 0° is an equatorial orbit that includes the spacecraft motion in the direction of the Moon's rotation and orbit

at inclination 180° follows an opposite direction to the rotation of the Moon. Both of these orbits have lower $J_{Optimal}$ of 1.723 km/s and 1.7315 km/s respectively.

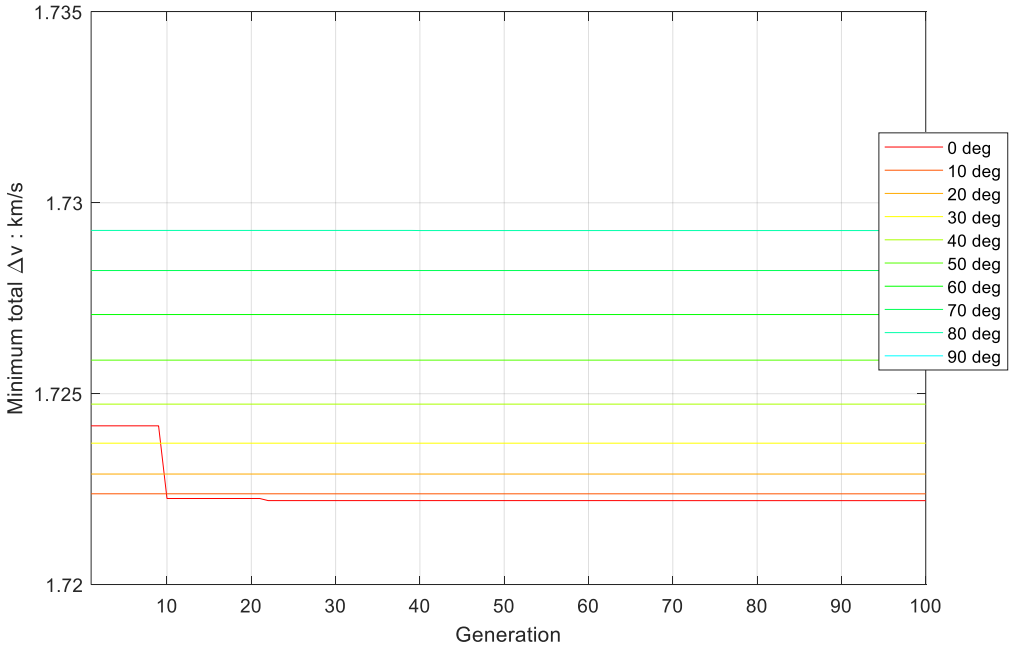

Figure 5.2: Sensitivity through a change in *i* for a landing site of ϕ=0° and λ=0° using initial conditions from Table 4.2 for prograde orbits.

It is to be noted that the PSO update starts at generation 1 in Fig. 5.1, 5.2 and Fig 5.3 with reference to the flowchart of PSO application to Lambert in Chapter 3. For results discussed in Chapter 4 in Case II, two more search space variables were added compared to Case I. This makes the analysis incomplete without investigating the dependency of other constant variables in $\bar{\zeta}_i^1$ for Case II. It was observed that using larger values of inclination for a landing site of ϕ=0° and λ=0°, increased $J_{Optimal}$ from 1.723 km/s at 10° to 1.74 km/s at 65° and around 2 km/s for retrograde orbits. Values of Ω or *u* corresponding to inclination values for Case II were higher at a lower inclination angle and went smaller for higher inclination angles. The values of Ω and *u* for the best

solutions in Case II, remained between 180° to 350°. This points to the fact that the ascending node is located in the opposite directional plane between the X-axis and the Z-axis in the MCI inertial frame. Time-to-land went lower for retrograde orbits at higher inclinations.

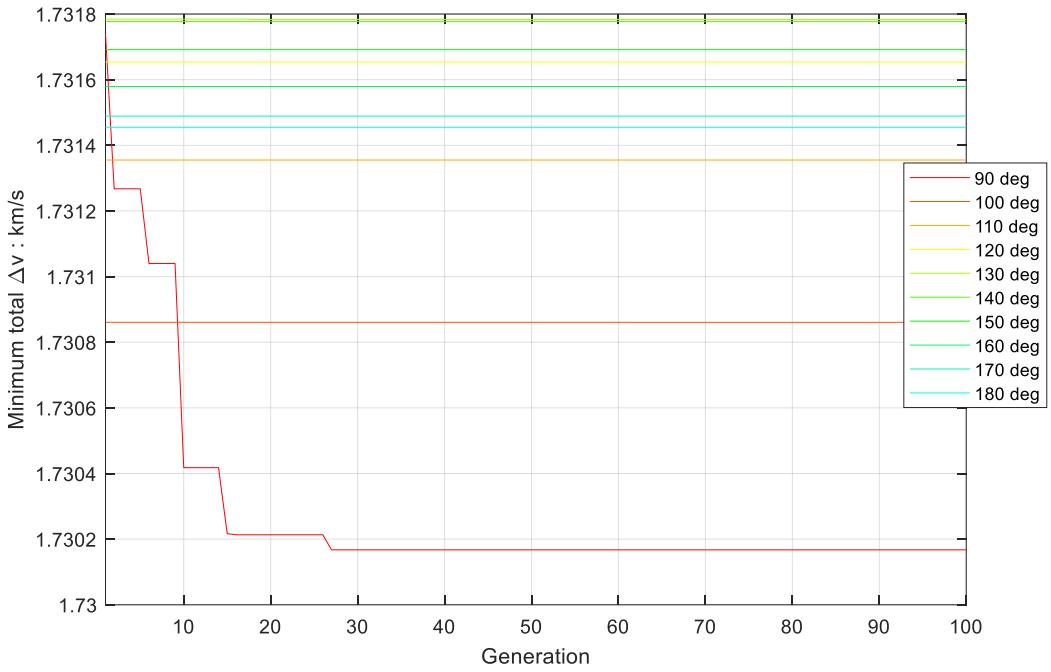

Figure 5.3: Sensitivity through a change in *i* for a landing site of ϕ=0° and λ=0° using initial conditions from Table 4.2 for retrograde orbits

5.1.2 Right ascension of ascending node of the orbit and the argument of latitude

Values of Ω and *u* that define the frame of the trajectory are analyzed for the initial conditions presented in Table 4.2 for Case I. Similar behavior to inclination in Fig. 5.2 and 5.3 were seen. It is evident from Fig 5.4 that values of $J_{Optimal}$ recorded, were higher for larger Ω and went lower for small values of Ω. This translates to the fact that when the ascending node is located

within 90° of the point of Aries in MCI frame, $J_{Optimal}$ remained less than 2.4 km/s. For values of Ω between 0° to 90°, $J_{Optimal}$ ranged from 2.9 km/s to 2.81 km/s and then went further lower to 1.89 km/s at Ω = 180°. This is directly relative to the angular difference between the right ascension of ascending node Ω and the longitude of the landing site.

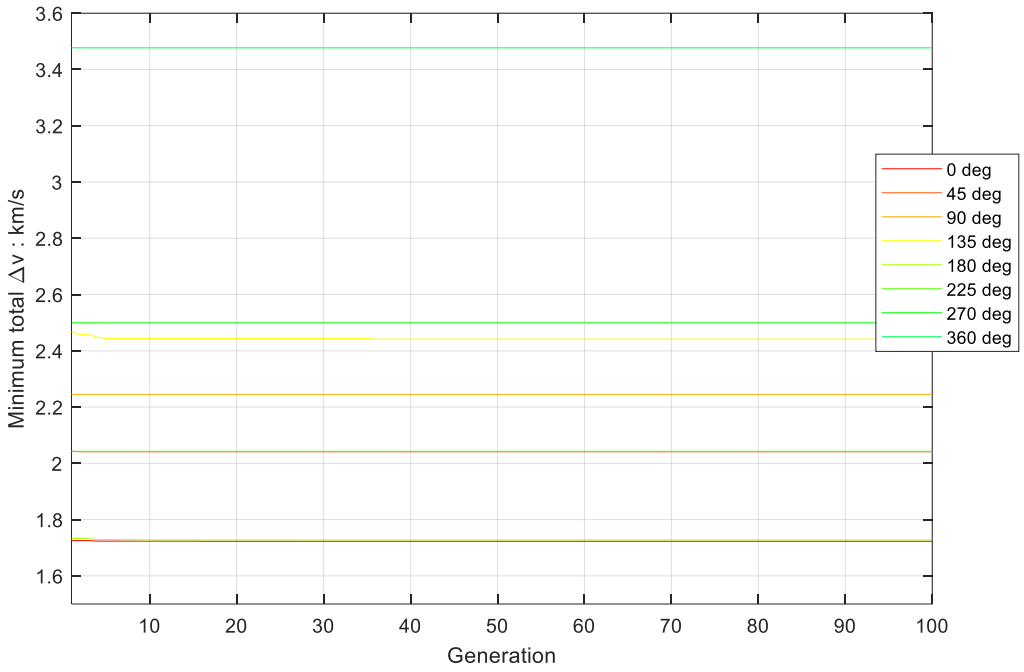

Figure 5.4: Sensitivity through a change in Ω for a landing site of ϕ=0° and λ=0° using initial conditions from Table 4.2

True anomaly and the argument of periapsis are not defined for circular orbits and so the argument of latitude was investigated. These results are included in Fig. 5.5 where $J_{Optimal}$ went lower for higher values of *u*. The horizontal axis in Fig. 5.5 is reduced to 10 generations to increase readability. Also not included in the graph is the value of $J_{Optimal}$ =2.941 km/s when u = 0°.

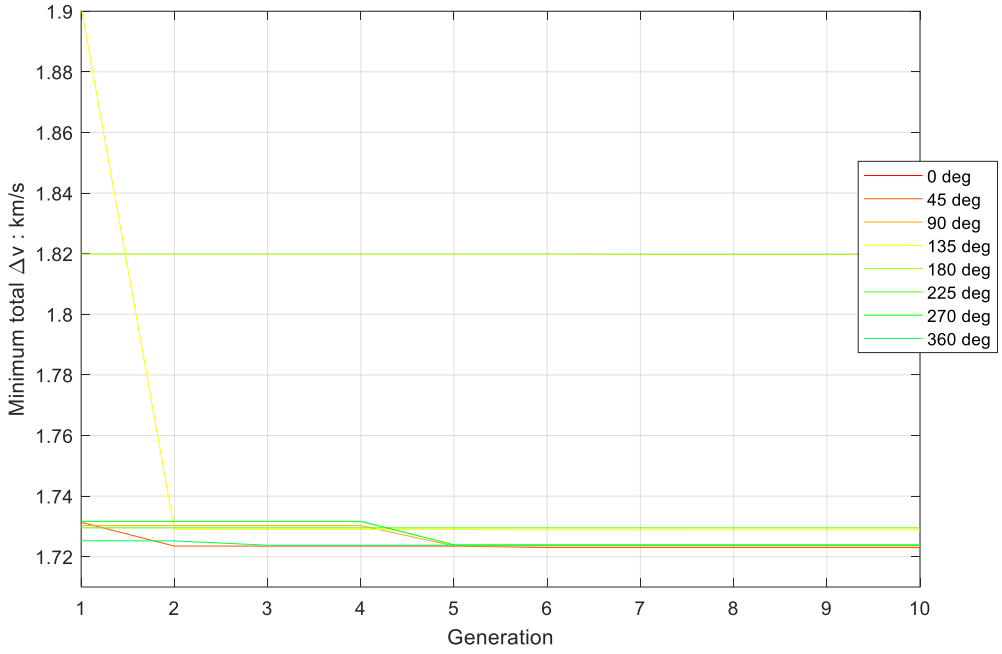

Figure 5.5: Sensitivity through change in *u* for a landing site of ϕ=0° and λ=0° using initial conditions from Table 4.2

Other than the Euler angles, the semi-major axis a, that affects the altitude and period of the orbit, is chosen based on the energy of the orbit. The energy of an orbit is inversely proportional to the semi-major axis and so for higher altitudes, with a higher semi-major axis, energy is less negative, and more energy is required for the orbital transfers. Equation 5.1 relates the energy of an orbit to the semi-major axis a, where μ is the standard gravitational parameter of the Moon and its value is 4904.8695 km^3/s^2.

$$\varepsilon = -\frac{\mu}{2a} \tag{5.1}$$

5.2 Landing Site Selection

The choice of landing site coordinates did not affect the $J_{Optimal}$ in Case I, but affected the time-to-land *T*, corresponding to the initial inclination value of the orbit selected. Note that if inclination was lower for smaller values of ϕ and λ, the time-to-land and the $J_{Optimal}$ were also lower compared to highly inclined orbits. This statement if used without a unique combination of Ω and θ or *u*, can be incorrect and that is where analysis in Case II helps. Analysis in Case II helps to find unique combinations of the variables in $\bar{\zeta}$ to land at the selected landing site. Besides, the terrain features considered partially for this analysis and inclination, time-to-land can also affect the landing site selection. For a small amount of propellant usage, more *T* can be required to land at a site through a higher orbital phase change maneuver and so selecting the right landing site becomes inevitable.

When a different landing site was picked for Case II, another combination of the variables in $\bar{\zeta}$ leads to $J_{Optimal}$. Out of them, the Apollo 11 landing site, "Mare Tranquillitatis" crater was selected and the ground track for landing at this site starting at initial conditions in Table 4.3 is illustrated in Fig. 5.6. The starting point of this ground track is ϕ =34° S and λ=112.9° W and reaches ϕ =0.67408° N and λ=23.47297° E in 2351.8 seconds. Note that, the ground track presented in Fig. 5.5 represents trajectory 1 at $J_{Optimal}$ and the other 9 trajectories also followed similar tracks to Fig 5.5 and can be compared to Fig. 4.19 in all.

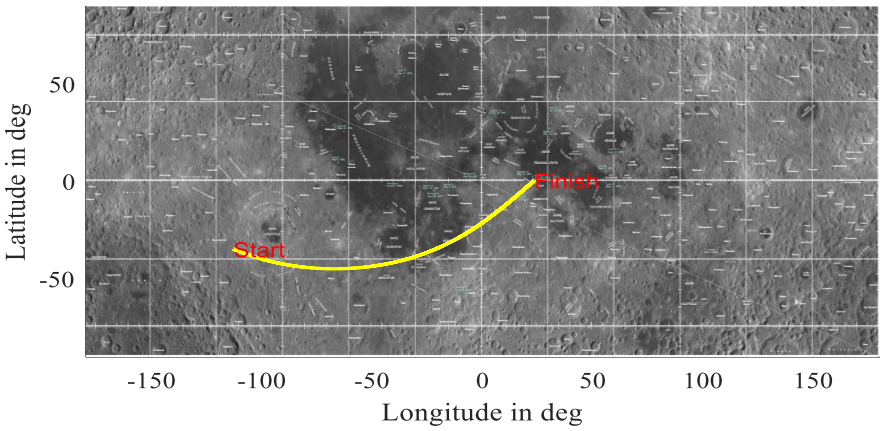

Figure 5.6: Ground track for the Apollo 11 landing site.

5.3 Number of Generations

The analysis in Chapter 4 used different numbers of generations for Case I and Case II. The Pareto frontier graphs in Fig. 4.4 and Fig 4.13, marked the convergence of cost function and when values of J stopped changing from generation to generation after about 50 generations in Case I, and after 2000 generations in Case II. Along with the changes in cost function J, the values of T in Case I and the values of Ω, u and T corresponding to the trajectory involved in PSO were also tracked. In Case I, it changed within low tolerances but in Case II, values of Ω, u and T changed drastically after every 500 generations and so to investigate for false convergence, the number of iterations for results presented in Case II were increased. This became necessary since this is a stochastic algorithm that produces a random value of the variable at each iteration. This also assured the stability of the variables that defined the 10 best trajectories at the end of the optimization

process. The number of iterations did not change the $J_{Optimal}$ after 2000 generations within a tolerance of 10^{-3} for the corresponding values of search space variables. Stable values of Ω, u and T were observed for the 10 best trajectories selected at the end of Case II. Therefore, the maximum number of generations in Case I is kept 100 while in Case II, it increased to 5000.

Chapter 6

Conclusion and Recommendations

The objective of this research was to develop a method to complete optimal lunar landing, starting at some initial orbit, by using particle swarm optimization (PSO) through Lambert targeting. The goal was to minimize the total velocity needed to start the descent at an altitude of 100 km above the lunar surface and land at a pre-selected location. This was done by searching for a local and global minimum through a search space defined by the classical orbital elements that define the shape, size, and orientation of the trajectory and the time-to-land on the Moon. The classical orbital elements include the semi-major axis, the eccentricity of the orbit, inclination with respect to the Moon's equatorial plane, the location of the right ascension of ascending node, the argument of latitude and true anomaly. The semi-major axis and eccentricity define the size and shape of the orbit while the inclination, right ascension of ascending node, argument of latitude and true anomaly define the orientation and position of the spacecraft in orbit. To increase interdependence between generations, the PSO algorithm was modified and simple crossover and mutation techniques were used. The ten best trajectories were selected and used as seeds to create 90 new trajectories. The value of Δv_{Total} was computed for each of these trajectories and the ten lowest Δv_{Total} were selected while the remainder were discarded. This continued until the best that is the minimum Δv_{Total} did not change over several generations.

Through results and analysis presented in Chapters 4 and 5, it was concluded that keeping the search space limited to just time-to-land T resulted in $J_{Optimal}$ and Δv_{Total} for the ten trajectories picked at the end of optimization and enabled selection of the landing site. When the decision variables were expanded to classical orbital elements within a specific range, better prediction of a combination of variables in the update vector, $\bar{\zeta}$, for the desired landing site were made at $J_{Optimal}$ for similarly inclined orbits were noticed. Landing at ϕ =0° and λ=0°, the "Sinus

Medii" crater on the surface of the Moon occurred within 41.46 minutes in Case I where the initial orbit was perfectly circular, inclined at 20° from the equatorial reference frame of the Moon in MCI with argument of latitude as 50°, in the direction of spacecraft motion. The $J_{Optimal}$ recorded for this event was 1.723 km/s after 100 generations. Landing at the same location in Case II by extending the search space variables to include the right ascension of the ascending node and argument of latitude, produced similar $J_{Optimal}$ of 1.72239 km/s after 5000 generations at an initial orbit. The initial orbit presented was inclined at 10° to the Moon's equatorial plane, the ascending node was located at 0.46° from the point of Aries on the Moon and the argument of latitude was noted as 35.56°. The time-of-flight recorded for this event was 45.78 minutes and appropriate ground tracks were discussed in Chapter 4. Chapter 5 included a discussion of the initial conditions that might affect the process of Lambert's targeting through PSO. The initial conditions include the classical orbital elements that define the initial orbit, the number of generations and the selection of landing sites for Case I as well as for Case II.

It was concluded that landing at lower angular values of latitude and longitude produced ideal $J_{Optimal}$ at inclination lower than 20° to the equatorial plane of the Moon. Landing near the poles demanded larger values of Δv_{Total} and the time-to-land, depending on the initial conditions used. Selection of initial conditions for the orbital elements to produce optimal trajectories affected Case I results more when compared to the robustness in Case II. Since this is a stochastic algorithm and the goal was to find the optimal descent point for repeatable landings on the Moon, sensitivity analysis provided details on the elements that affected results. Values for the inclination angle and the right ascension of ascending node that defines the orientation of the transfer orbit with respect to the Moon, affected results the most. The values of $J_{Optimal}$ for both the cases are similar and compare well to the Hohmann transfer velocities of value 1.7492 km/s, assuming coplanarity between initial orbits. This indicates that the optimized Δv_{Total} reduced by 1.49 % to that of

Hohmann, for Case I and around the same for Case II. Reduction in Δv_{Total} also corresponds to the reduction in propellant usage.

For future research, this optimization can be used to explore other conic sections like elliptical, parabolic or hyperbolic trajectories for various maneuvers. By introducing different values of personal and social coefficients, changes in search space variables corresponding to $J_{Optimal}$ can be analysed. The personal and social coefficients are the constants that define the rate of change of the variables by scaling them with the local and global best value of that variable at that iteration. The initial conditions used play an important role in any optimization process and, hence, PSO could be used to provide sensitivity analysis on the initial orbit altitude. If this optimization is used to generate landing trajectories at another planetary surface, an appropriate atmospheric model needs to be introduced.

Many missions have been carried out to explore the Moon with some successful landings and some potential crashes and some lost contacts. In such times, when the space-faring nations are going back to the Moon to stay, explore and come back, it becomes inevitable for future generations to keep searching for optimal methods to explore the unknown, reach there, set up a habitat and continue expanding the horizons of knowledge.

References

[1] Northon, K. (2017, December 11). President Signs New Space Policy Directive. Retrieved from https://www.nasa.gov/press-release/new-space-policy-directive-calls-for-human-expansion-across-solar-system

[2] Northon, K. (2019, July 01). NASA Selects 12 New Lunar Science, Technology Investigations. Retrieved from https://www.nasa.gov/press-release/nasa-selects-12-new-lunar-science-technology-investigations

[3] Moon to Mars. (n.d.). Retrieved July 1, 2019, from https://www.nasa.gov/specials/Moon2mars/

[4] Young, A. (2017, March 23). SpaceX's sustainable space travel: Recycled rockets are green - and they slash launch costs, too. Retrieved from https://www.salon.com/2017/03/22/spacexs-sustainable-space-travel-recycled-rockets-could-slash-launch-costs-by-30-percent/

[5] (n.d.). Retrieved July 2, 2019, from http://www.space-settlement-institute.org/private-space-companies.html

[6] Epp, C. D., Robertson, E. A., & Brady, T. (2008). Autonomous Landing and Hazard Avoidance Technology (ALHAT). 2008 IEEE Aerospace Conference. DOI:10.1109/aero.2008.4526297

[7] Pontani, M., & Conway, B. A. (2010). Particle Swarm Optimization Applied to Space Trajectories. *Journal of Guidance, Control, and Dynamics, 33*(5), 1429-1441. DOI:10.2514/1.48475

[8a] Eberhart, R., & Kennedy, J. (1995). A new optimizer using particle swarm theory. *IEEE, MHS'95. Proceedings of the Sixth International Symposium on Micro Machine and Human Science*.

[8b] Kennedy, J., & Eberhart, R. (1995). Particle Swarm Optimization. *IEEE*.

[9] Bessette, C. R., & Spencer, D. B. (2007). Performance Comparison of Stochastic Search Algorithms on the Interplanetary Gravity-Assist Trajectory Problem. *Journal of Spacecraft and Rockets, 44*(3), 722-724. DOI:10.2514/1.25718

[10] Couceiro, M., & Ghamisi, P. (2016). Fractional Order Darwinian Particle Swarm Optimization. *SpringerBriefs in Applied Sciences and Technology*. DOI:10.1007/978-3-319-19635-0

[11] Pontani, M., Ghosh, P., & Conway, B. A. (2012). Particle Swarm Optimization of Multiple-Burn Rendezvous Trajectories. *Journal of Guidance, Control, and Dynamics,35*(4), 1192-1207. DOI:10.2514/1.55592

[12] Pontani, M. (2014). Particle swarm optimization of ascent trajectories of multistage launch vehicles. *Acta Astronautica,94*(2), 852-864. DOI: 10.1016/j.actaastro.2013.09.013

[13] Jiang, X., & Li, S. (2015). Mars atmospheric entry trajectory optimization via particle swarm optimization and Gauss pseudo-spectral method. *Proceedings of the Institution of Mechanical Engineers, Part G: Journal of Aerospace Engineering,230*(12), 2320-2329. DOI:10.1177/0954410015622230

[14] Vallado, D. (1996). *Fundamentals of Astrodynamics and Applications* (First ed., Space Technology Series). Mc Graw Hill.

[15] Curtis, H. D. (2010). *Orbital Mechanics for Engineering Students*. Amsterdam: Elsevier, Butterworth-Heinemann.

[16] Escobal, P. R. (1978). *Methods of orbit determination*. Huntington, NY: Robert E. Krieger.

[17] (2012, January 12). Retrieved July 2, 2019, from https://eclipse.gsfc.nasa.gov/SEhelp/Moonorbit.html

[18] Bryson, A. E., & Ho, Y. (1975). *Applied Optimal Control: Optimization, estimation, and control*. Levittown, PA: Taylor & Francis

[19] Russell, R. P., & Lara, M. (2007). Long-Lifetime Lunar Repeat Ground Track Orbits. *Journal of Guidance, Control, and Dynamics, 30*(4), 982-993. DOI:10.2514/1.27104

[20] Biesbroek, R., & Janin, G. (2000). Ways to the Moon? *ESA Bulletin 103 — August 2000*.

[21] Hu, X., Eberhart, R., & Shi, Y. (n.d.). Engineering optimization with particle swarm. *Proceedings of the 2003 IEEE Swarm Intelligence Symposium. SIS03 (Cat. No.03EX706)*. DOI:10.1109/sis.2003.1202247

[22] Davies, M. E., & Colvin, T. R. (2000). Lunar coordinates in the regions of the Apollo landers. *Journal of Geophysical Research: Planets, 105*(E8), 20277-20280. DOI:10.1029/1999je001165

[23] (n.d.). Retrieved July 2, 2019, from https://www.nhc.noaa.gov/gccalc.shtml

[24] Tapley, B. D., Schutz, B. E., & Born, G. H. (2004). *Statistical orbit determination*. Amsterdam: Elsevier.

[25] Battin, R. H. (1987). *An introduction to the mathematics and methods of astrodynamics*. Reston, VA: AIAA, American Institute of Aeronautics and Astronautics.

[26] De Jong, K. (2006). *Evolutionary Computation A Unified Approach*. Bradford Books.

[27] Mendell, W. W. (1986). *Lunar Bases and Space Activities of the 21st Century*. Lunar and Planetary Institute Houston.

[28] Hare, T.M., Hayward, R. K., Blue, J. S., Archinal, B. A., Robinson, M. S., Speyerer, E. J., Mazarico, E. (2015). *Image map of the Moon [Prepared for National Aeronautics and Space Administration by U.S. Geological Survey]*. Retrieved July 9, 2019.

[29] Engelbrecht, A. P. (2007). *Computational Intelligence. An Introduction* (2nd ed.). Hoboken, NJ: Wiley.

Appendix

This section outlines the procedures followed in MATLAB for Lambert targeting through PSO. With more information on the variables from Chapter 2 and Chapter 3, Sections A, B and C presents the dependency on coordinate transformation, PSO optimization and Lambert's solution. Algorithms A, B and C are connected in sequential order.

A. Initial orbit determination and evaluating cost function for spacecraft

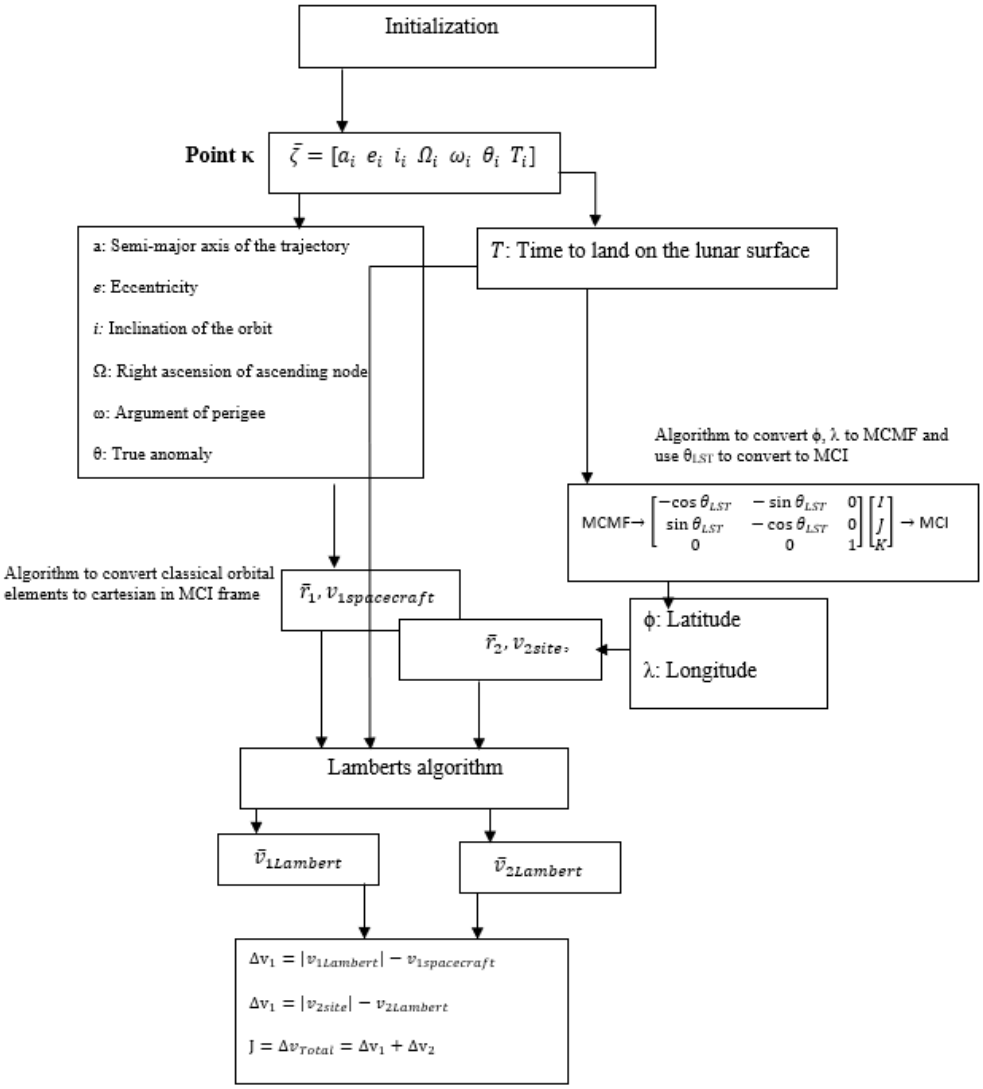

B. PSO on Lambert and extremity check for decision variables

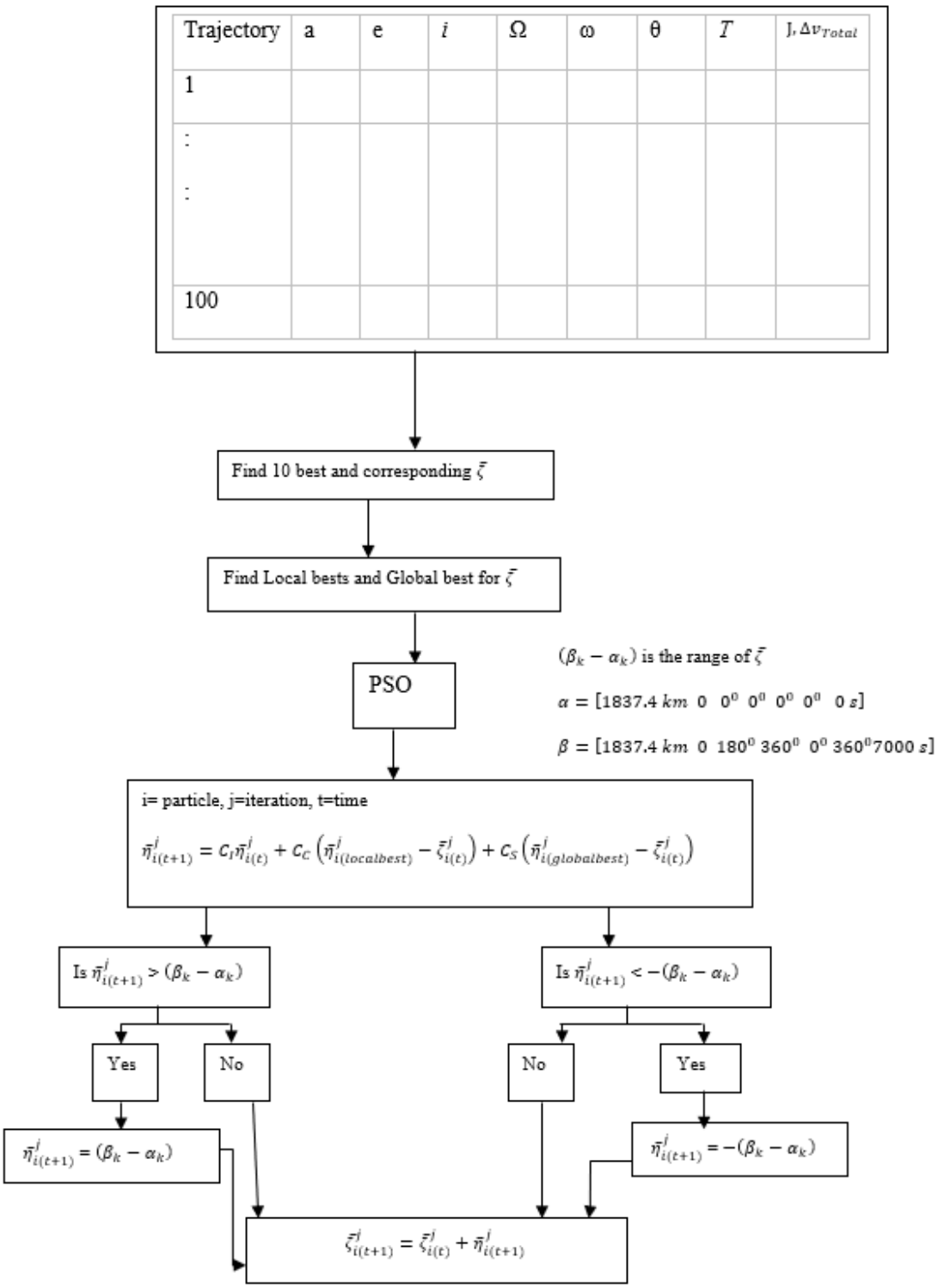

C. Extremity check for PSO update variable $\bar{\eta}$ and creation of the next generation.